VOLUME 32 | SUPPLEMENT 2 | MARCH 2019

MODERN PATHOLOGY

USCAP 2019

ABSTRACTS

MEDICAL RENAL PATHOLOGY (INCLUDING TRANSPLANTATION) (1581-1620)

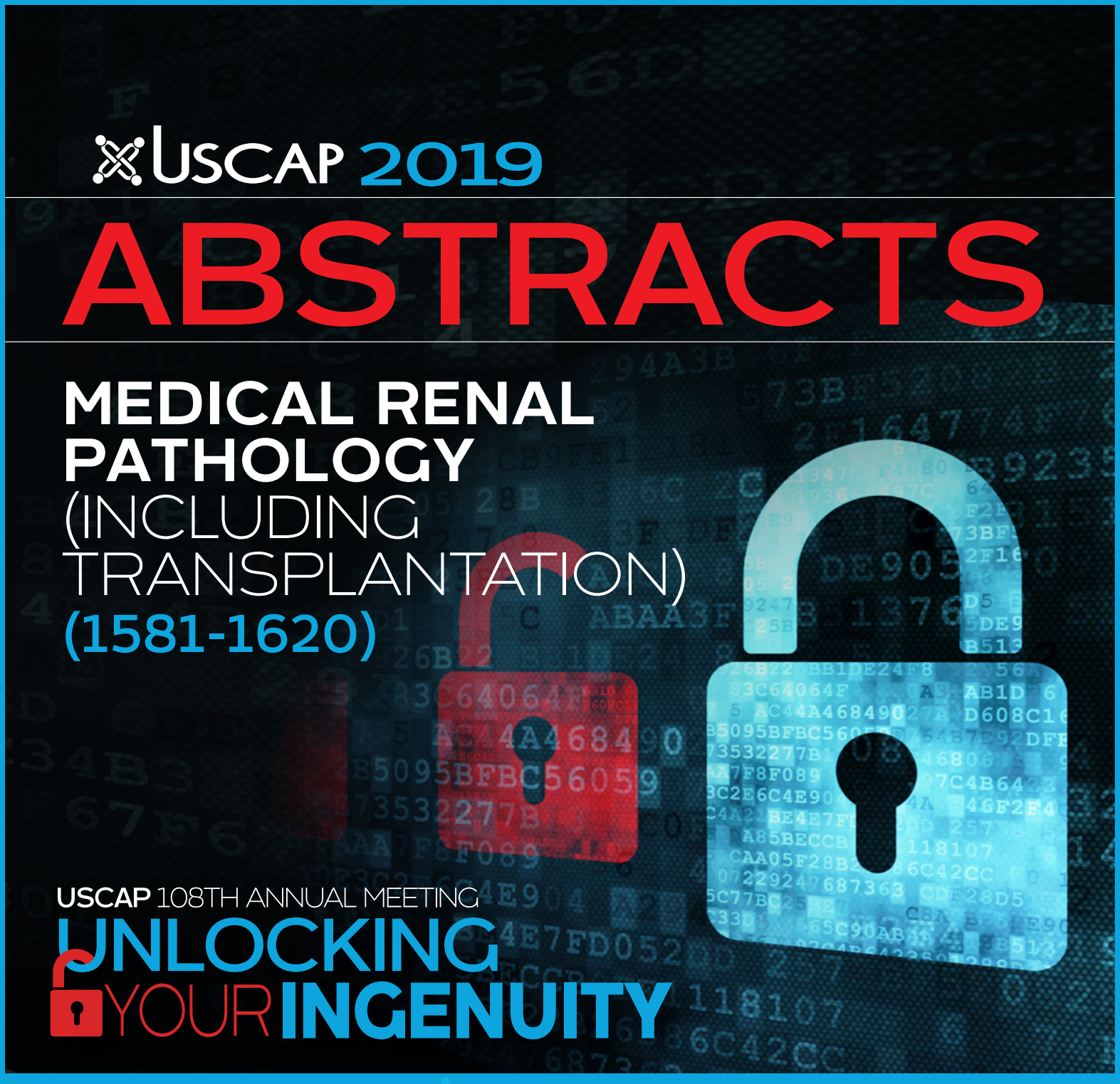

USCAP 108TH ANNUAL MEETING

UNLOCKING YOUR INGENUITY

MARCH 16-21, 2019

National Harbor, Maryland
Gaylord National Resort & Convention Center

Published by
SPRINGER NATURE
www.ModernPathology.org

USCAP Creating a Better Pathologist
AN OFFICIAL JOURNAL OF THE UNITED STATES AND CANADIAN ACADEMY OF PATHOLOGY

EDUCATION COMMITTEE

Jason L. Hornick, Chair
Rhonda K. Yantiss, Chair, Abstract Review Board and Assignment Committee
Laura W. Lamps, Chair, CME Subcommittee
Steven D. Billings, Interactive Microscopy Subcommittee
Shree G. Sharma, Informatics Subcommittee
Raja R. Seethala, Short Course Coordinator
Ilan Weinreb, Subcommittee for Unique Live Course Offerings
David B. Kaminsky (Ex-Officio)
Aleodor (Doru) Andea
Zubair Baloch
Olca Basturk
Gregory R. Bean, Pathologist-in-Training
Daniel J. Brat
Ashley M. Cimino-Mathews
James R. Cook
Sarah M. Dry
William C. Faquin
Carol F. Farver
Yuri Fedoriw
Meera R. Hameed
Michelle S. Hirsch
Lakshmi Priya Kunju
Anna Marie Mulligan
Rish Pai
Vinita Parkash
Anil Parwani
Deepa Patil
Kwun Wah Wen, Pathologist-in-Training

ABSTRACT REVIEW BOARD

Benjamin Adam
Michelle Afkhami
Narasimhan (Narsi) Agaram
Rouba Ali-Fehmi
Ghassan Allo
Isabel Alvarado-Cabrero
Christina Arnold
Rohit Bhargava
Justin Bishop
Jennifer Boland
Elena Brachtel
Marilyn Bui
Shelley Caltharp
Joanna Chan
Jennifer Chapman
Hui Chen
Yingbei Chen
Benjamin Chen
Rebecca Chernock
Beth Clark
James Conner
Alejandro Contreras
Claudiu Cotta
Timothy D'Alfonso
Farbod Darvishian
Jessica Davis
Heather Dawson
Elizabeth Demicco
Suzanne Dintzis
Michelle Downes
Daniel Dye
Andrew Evans
Michael Feely
Dennis Firchau
Larissa Furtado
Anthony Gill
Ryan Gill
Paula Ginter
Tamara Giorgadze
Raul Gonzalez
Purva Gopal
Anuradha Gopalan
Jennifer Gordetsky
Rondell Graham
Alejandro Gru
Nilesh Gupta
Mamta Gupta
Krisztina Hanley
Douglas Hartman
Yael Heher
Walter Henricks
John Higgins
Mai Hoang
Mojgan Hosseini
Aaron Huber
Peter Illei
Doina Ivan
Wei Jiang
Vickie Jo
Kirk Jones
Neerja Kambham
Chiah Sui (Sunny) Kao
Dipti Karamchandani
Darcy Kerr
Ashraf Khan
Rebecca King
Michael Kluk
Kristine Konopka
Gregor Krings
Asangi Kumarapeli
Alvaro Laga
Cheng-Han Lee
Zaibo Li
Haiyan Liu
Xiuli Liu
Yan-Chun Liu
Tamara Lotan
Anthony Magliocco
Kruti Maniar
Jonathan Marotti
Emily Mason
Jerri McLemore
Bruce McManus
David Meredith
Anne Mills
Neda Moatamed
Sara Monaco
Atis Muehlenbachs
Bita Naini
Dianna Ng
Tony Ng
Ericka Olgaard
Jacqueline Parai
Yan Peng
David Pisapia
Alexandros Polydorides
Sonam Prakash
Manju Prasad
Peter Pytel
Joseph Rabban
Stanley Radio
Emad Rakha
Preetha Ramalingam
Priya Rao
Robyn Reed
Michelle Reid
Natasha Rekhtman
Michael Rivera
Michael Roh
Andres Roma
Avi Rosenberg
Esther (Diana) Rossi
Peter Sadow
Safia Salaria
Steven Salvatore
Souzan Sanati
Sandro Santagata
Anjali Saqi
Frank Schneider
Jeanne Shen
Jiaqi Shi
Wun-Ju Shieh
Gabriel Sica
Deepika Sirohi
Kalliopi Siziopikou
Lauren Smith
Sara Szabo
Julie Teruya-Feldstein
Gaetano Thiene
Khin Thway
Rashmi Tondon
Jose Torrealba
Evi Vakiani
Christopher VandenBussche
Sonal Varma
Endi Wang
Christopher Weber
Olga Weinberg
Sara Wobker
Mina Xu
Shaofeng Yan
Anjana Yeldandi
Akihiko Yoshida
Gloria Young
Minghao Zhong
Yaolin Zhou
Hongfa Zhu
Debra Zynger

1581 The Molecular Pathology of Immune Checkpoint Inhibitor-Induced Acute Kidney Injury: Overlap between Native and Transplant Phenotypes

Benjamin Adam[1], Christie Boils[2], Lihong Bu[3], Karine Renaudin[4], Michael Mengel[1]
[1]University of Alberta, Edmonton, AB, [2]Arkana Laboratories, Little Rock, AR, [3]University of Minnesota, Minneapolis, MN, [4]Service Anatomie Pathologique, Nantes, France

Disclosures: Benjamin Adam: None; Christie Boils: None; Lihong Bu: None; Karine Renaudin: None; Michael Mengel: None

Background: Immune checkpoint inhibitor (ICI) therapy has shown survival benefit in a growing number of malignancies. However, due to their immunostimulatory mechanism of action, ICIs have been associated with numerous autoimmune and alloimmune adverse events, including acute interstitial nephritis (AIN) in native kidneys and acute T-cell mediated rejection (TCMR) in transplant kidneys. The goal of this study was to further characterize these adverse events through comparative molecular analysis.

Design: NanoString was used to measure the expression of 800 genes in 25 archival kidney biopsies. The genes included a 770-gene PanCancer Immune Profiling Panel plus 30 additional TCMR-related genes. The samples included native kidney biopsies with ICI-related AIN (ICI-AIN, n=2), ICI-related crescentic glomerulonephritis (ICI-CGN, n=1) and non-ICI-related AIN (AIN, n=4); transplant kidney biopsies with ICI-related TCMR (ICI-TCMR, n=2) and non-ICI-related TCMR (TCMR, n=8); and normal implantation biopsies (Normal, n=8). Exploratory analysis was performed using principal component analysis (PCA) and heat maps with hierarchical clustering. Gene sets associated with TCMR and AIN were identified using volcano plot analysis with a false discovery rate (FDR) threshold of 0.05. Mann-Whitney U-test was used to compare gene set expression between groups.

Results: Unsupervised PCA and heat map analysis demonstrated distinct clustering of Normal, AIN and TCMR biopsies based on gene expression (**Figure 1**). ICI-AIN overlapped with AIN while, interestingly, ICI-TCMR clustered more closely with AIN than TCMR. 341 genes were significantly upregulated in TCMR vs. Normal and AIN, and 111 genes were upregulated in AIN vs. Normal and TCMR (FDR<0.05); the top 100 of each were combined into aggregate TCMR and AIN gene sets, respectively. TCMR gene set expression was higher in TCMR than AIN (p=0.048) but there was no significant difference between ICI-TCMR and ICI-AIN, and no difference between the ICI groups and TCMR or AIN (**Figure 2**). AIN gene set expression was higher than TCMR in AIN, ICI-AIN and ICI-TCMR (p<0.044) but there was no significant difference between these three groups.

Figure 1 - 1581

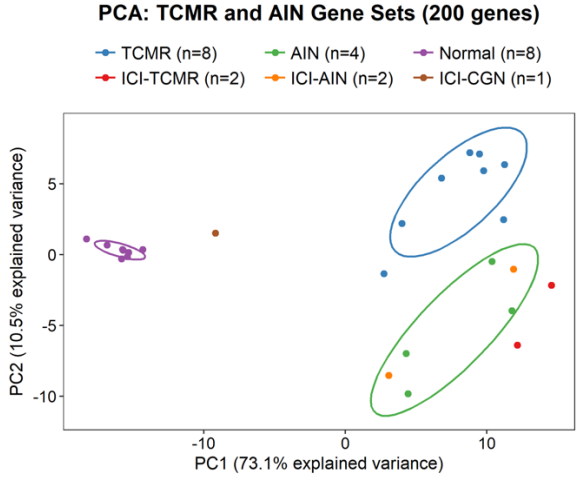

Figure 2 - 1581

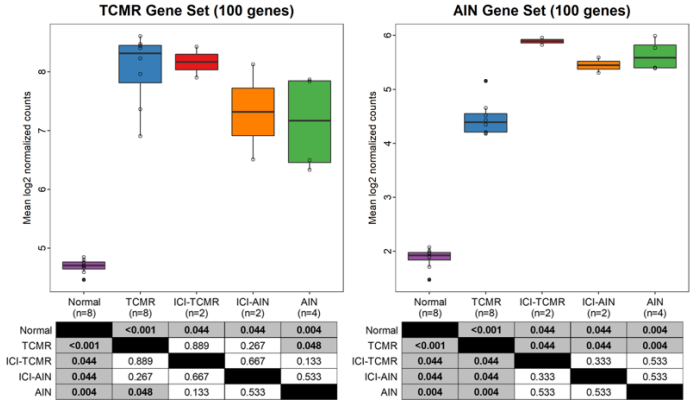

	Normal (n=8)	TCMR (n=8)	ICI-TCMR (n=2)	ICI-AIN (n=2)	AIN (n=4)
Normal		<0.001	0.044	0.044	0.004
TCMR	<0.001		0.889	0.267	0.048
ICI-TCMR	0.044	0.889		0.667	0.133
ICI-AIN	0.044	0.267	0.667		0.533
AIN	0.004	0.048	0.133	0.533	

	Normal (n=8)	TCMR (n=8)	ICI-TCMR (n=2)	ICI-AIN (n=2)	AIN (n=4)
Normal		<0.001	0.044	0.044	0.004
TCMR	<0.001		0.044	0.044	0.004
ICI-TCMR	0.044	0.044		0.333	0.533
ICI-AIN	0.044	0.044	0.333		0.533
AIN	0.004	0.004	0.533	0.533	

Conclusions: These results suggest that ICI-AIN and ICI-TCMR both have molecular phenotypes closer to AIN than TCMR. In ICI-TCMR, this may reflect non-specific activation of the immune system compared with a more specific alloimmune response in TCMR. These findings may facilitate improved understanding and management of these adverse events.

1582 Clinical, Pathological and HLA Typing of Membranous Nephropathy (MN) in Renal Allografts

Ibrahim Batal[1], Vasilescu Elena[2], Dominick Santoriello[2], Satoru Kudose[3], Syed Husain[1], Andrew Bomback[1], Michael Stokes[4], Vivette D'Agati[5], Glen Markowitz[6]
[1]Columbia University, New York, NY, [2]New York-Presbyterian/Columbia University Medical Center, New York, NY, [3]New York, NY, [4]Columbia University College of Physicians and Surgeons, New York, NY, [5]Tenafly, NJ, [6]Columbia Presbyterian Medical Center, Tarrytown, NY

Disclosures: Ibrahim Batal: None; Vasilescu Elena: None; Dominick Santoriello: None; Satoru Kudose: None; Syed Husain: None; Andrew Bomback: None; Michael Stokes: None; Vivette D'Agati: None; Glen Markowitz: None

Background: In the native kidney, patients with molecular tissue typing for HLA-DQA1*05:01/DQB1*02:01 (which corresponds to a proportion of subjects with HLA-DQ2 by serologic typing) are at increased risk for developing PLA2R+ MN. Post-kidney transplant (post-KTx) MN is understudied. We present our experience with post-KTx MN, focusing on the association between PLA2R status and HLA-DQ2 typing.

Design: Clinicopathologic characteristics, PLA2R status, and HLA typing of donors and recipients from 30 cases of post-KTx MN treated at our institution between 2005-2018 were studied. A cohort of 17 recipients with ESRD secondary to MN and HLA-DQ2 was also followed to assess the significance of donor HLA-DQ2 in predicting recurrence of MN.

Results: Patients with post-KTx MN (n=30) were 43 ±16 year-old and included 23% women, 20% African American, and 43% recipients of deceased donor grafts. Index biopsies were obtained 869 ± 1305 days post-transplantation with concurrent serum creatinine of 2.6 ± 2.1 mg/dl and proteinuria of 2.7 ± 2.7 g/day. Proteinuria levels, segmental sclerosis, and transplant glomerulopathy were associated with inferior graft survival.
PLA2R status was available for 27 patients (all in tissue except 1 in the serum). PLA2R$^+$ MN (n=11) included 8 (73%) recurrent disease, 1 (9%) de novo, and 2 (18%) uncertain (unknown end stage renal disease; ESRD). In contrast, PLA2R$^-$ MN (n=16) included 9 (56%) de novo disease, 6 (38%) recurrent, and 1 (6%) uncertain. When tissue typing was available, recipients with PLA2R$^+$ MN had numerically higher prevalence of HLA-DQ2 than recipients with PLA2R$^-$ MN [5/10 (50%) vs. 3/13 (23%), P=0.2]. Importantly, recipients with PLA2R$^+$ MN were also more likely to have received grafts from HLA-DQ2 donors compared to recipients with PLA2R- MN [7/8 (88%) vs. 3/14 (21%), P=0.006].
Among a larger cohort of 17 patients with DQ2 and ESRD secondary to MN, recurrent MN was seen in 7/9 DQ2$^+$ donor kidneys but only 1/8 DQ2$^-$ donor kidneys, resulting in 88% sensitivity and 78% specificity for predicting recurrence of MN (Table).

Recipients with DQ2 and ESRD due to MN		
	Rerurrence of MN (n=8)	No recurrence of MN (n=9)
Donors positive for DQ2 (n=9)	7	2
Donors negative for DQ2 (n=8)	1	7

Conclusions: In the kidney allograft, positive PLA2R is more common in recurrent than de novo MN. Post-KTx PLA2R$^+$ MN is tightly linked to HLA-DQ2 in the donor, which may influence pre-transplant allocation of kidney allografts.

1583 Alloimmunity Significantly Influences Worse Outcome after Deceased Donor Renal Transplantation (DRTx)

Ibrahim Batal[1], Geo Serban[2], Mohan Sumit[3], Syed Husain[1], Shana Coley[1], Vasilescu Elena[3], Vivette D'Agati[4], Glen Markowitz[5], Lloyd Ratner[3]
[1]Columbia University, New York, NY, [2]Columbia Medical Center, Bronx, NY, [3]New York-Presbyterian/Columbia University Medical Center, New York, NY, [4]Tenafly, NJ, [5]Columbia Presbyterian Medical Center, Tarrytown, NY

Disclosures: Ibrahim Batal: None; Geo Serban: None; Mohan Sumit: None; Syed Husain: None; Shana Coley: None; Vasilescu Elena: None; Vivette D'Agati: None; Glen Markowitz: None; Lloyd Ratner: None

Background: Regardless of donor histologic changes, long-term outcome is inferior following DRTx compared to living donor renal transplantation (LRTx). We have shown that ischemia-reperfusion injury (IRI), which is more pronounced in DRTx, is associated with accelerated activation and very early emigration of donor dendritic cells (DCs) out of the allograft. We explore the reasons behind the difference in outcome between DRTx and LRTx with special focus on alloimmunity.

Design: (1) A cohort of 696 consecutive kidney allograft recipients (336 LRTx, 360 DRTx), who underwent kidney transplant between 1/2006-12/2009 with available post-reperfusion biopsies were followed up for 65±36 months. Post-reperfusion biopsies were classified according to donor chronic histologic changes as “optimal” vs. “suboptimal” as previously described (suboptimal if any of the following: >10% glomerulosclerosis, >10% tubulointerstitial scarring or >mild vascular sclerosis).

(2) RNA was isolated from 15 formalin-fixed paraffin embedded post-reperfusion biopsies and RNA expression was compared between LRTx (n=6) vs. DRTx (n=9) using multiplexed color-coded probe-based gene expression profiling (Nanostring, Seattle, WA).

Results: Compared to LRTx (n=336), DRTx (n=360) had more acute rejection episodes (P<0.001) and worse allograft survival (p<0.001). Compared to LRTx *with optimal histology* (n=213), DRTx *with optimal histology* (n=166) had similar rejection episodes (P=0.57) but worse allograft survival (P=0.001). In contrast, DRTx *with suboptimal histology* (n=194) had more rejection episodes and worse allograft survival as compared to their LRTx counterparts *with suboptimal histology*(n=123, P<0.001 in each) **(Figure 1)**.

Despite the small sample size used for gene expression studies, 216/770 genes showed significant expression differences between DRTx and LRTx. Genes related to activation of complement pathways and diverse leukocyte functions, including DC activation, were upregulated in DRTx **(Figure 2)**. This overall increased DC gene expression in DRTx was seen despite lower DC density in DRTx post-reperfusion biopsies as measured using BDCA1 immunoperoxidase staining, likely secondary to accelerated DC emigration from DRTx allografts (DRTx: 0.5 ±0.4 vs. LRTx 1.1 ±0.5 cells/hpf, P=0.01).

Figure 1 - 1583

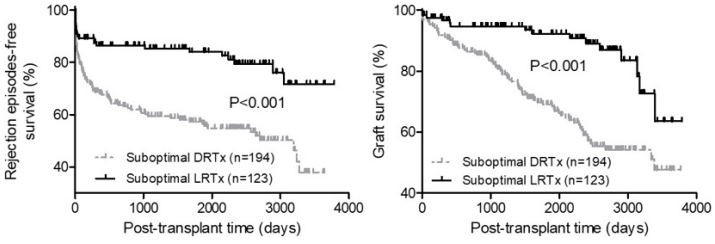

Figure 2 - 1583

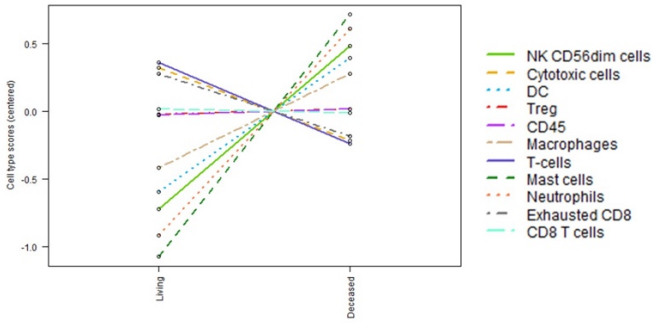

Conclusions: Compared LRTx, DRTx show increased alloimmunity secondary to IRI and donor DC activation. In the presence of *suboptimal histology*, this would manifest histologically as more rejection episodes that may adversely affect prognosis.

1584 Monoclonal Gammopathies of Renal Significance with Clinical Correlation

Angela Bayly[1], Levina Dear[2], David Brown[1], Brian Nankivell[1], Seethalakshmi Viswanathan[3]
[1]Westmead Hospital, Westmead, NSW, Australia, [2]Westmead Hospital, Sydney, NSW, Australia, [3]Sydney, NSW, Australia

Disclosures: Angela Bayly: None; Levina Dear: None; David Brown: None; Brian Nankivell: None; Seethalakshmi Viswanathan: None

Background: Monoclonal gammopathies of renal significance (MGRS) are a clinically significant group of disorders that may lead to end-organ damage without prompt diagnosis and management. MGRS encompasses multiple entities, including light chain amyloidosis, fibrillary glomerulonephritis, monoclonal immunoglobulin deposition disease (MIDD) and cryoglobulinemic glomerulonephritis. In this study, we sought to characterise and compare the clinical and morphologic findings in each disease.

Design: Renal biopsies with a diagnosis of MGRS were retrospectively reviewed at a tertiary referral institution over a five year period, from January 2012 to December 2016. The biopsies were studied by light microscopy, including special stains, immunofluorescence and electron microscopy. Clinical data, where available, was also reviewed and included renal and haematological parameters, underlying aetiological factors and outcome data.

Results: A total of 55 cases were identified, 37 males and 18 females. The mean age was 66 years.

AL amyloid was the most frequent pathology seen and accounted for 58% of cases, followed by fibrillary GN (18%), MIDD (12%) and cryoglobulinemia (7%). Chronicity was assessed by degree of fibrosis and percentage of sclerosed glomeruli and biopsies showed a mean of 25% globally sclerosed glomeruli (AL amyloid cases 32%, fibrillary GN 25%, MIDD 15%, cryoglobulinemic GN 0%).

The cases of MIDD showed variable light microscopy findings and included nodular sclerosis, membranoproliferative glomerulonephritis and membranous glomerulopathy. Of those with available clinical information 43% were diagnosed with multiple myeloma.

Follow up data was available in 43 patients (78%) and ranged from 1 to 64 months. Primary outcome was based on overall or renal survival. At a follow up of 60 months, 48% of patients had developed renal failure and 56% of patients had died. There was no significant difference in outcome in patients with amyloid, fibrillary GN or MIDD.

Figure 1 - 1584

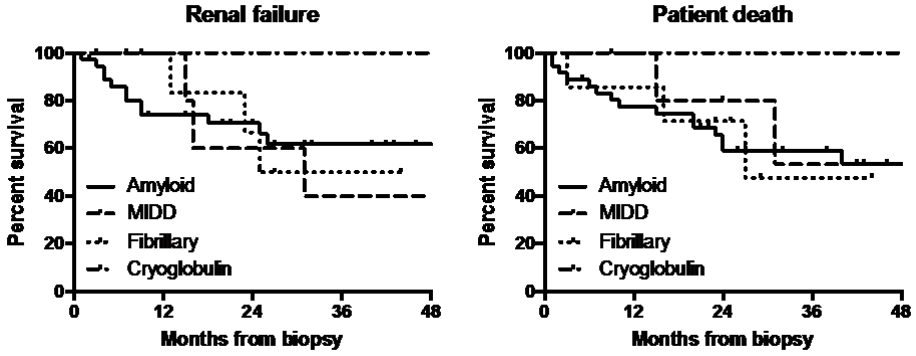

Conclusions: MGRS cases seen included light chain amyloidosis, fibrillary GN, MIDD and cryoglobulinemic GN. No significant difference in outcome was seen in patients with amyloid, fibrillary GN or MIDD. The cases of MIDD showed variable light microscopy features, mimicking other glomerulonephritides and may be the first presentation of an underlying haematological malignancy.

1585 Lupus Nephritis Histopathological Classification and Clinical Manifestations: A Retrospective Review in a South African Referral Centre

Adam Botha[1], Pulane Mosiane[2]
[1]University of the Witwatersrand/National Health Laboratory Service, Johannesburg, South Africa, [2]National Health Laboratory Services, Johannesburg, South Africa

Disclosures: Adam Botha: None; Pulane Mosiane: None

Background: Lupus nephritis (LN) is an important complication of systemic lupus erythematosus (SLE), which is increasingly being diagnosed in the diverse population of South Africa. Renal failure as a result of LN has been reported as the second commonest cause of death in South African patients with SLE.

There is a paucity of recent literature detailing the distribution of LN histopathological classes and their associations in Johannesburg, South Africa's most populous city. This study aims to describe these features.

Design: A retrospective laboratory report review was performed on cases of renal biopsy-proven LN in adults at a single anatomical pathology referral laboratory in Johannesburg over a 1-year period.

Results: From a total of 461 renal biopsies analysed in the centre, 22% (N=100) were performed in patients with SLE. Of these, 20 were excluded due to age, inadequate tissue or missing data. 80 cases of LN were included.

Of these, 76 were female (95%) and 4 (5%) were male. The mean age was 31.4 years (±8.9). The commonest class of LN was International Society of Nephrology (ISN) / Renal Pathology Society (RPS) class IV (36%), followed by class III (32%), pure class V (15%), class II (8%), class I (5%) and class VI (4%).

Combined class III + V comprised 50% of cases of class III LN, while combined class IV + V comprised 45% of class IV LN. All combined classes represented 33% of the total number of cases.

The commonest clinical presentations were sub-nephrotic proteinuria (43%), renal dysfunction (low eGFR) (41%), nephrotic syndrome (25%) and combined haematuria and proteinuria (11%). The majority of cases (53%) with proliferative LN (class III and IV) presented with renal dysfunction, accounting for 91% of the total cases that presented with renal dysfunction.

Conclusions: The demographic data as well as frequencies of the different ISN/RPS classes of LN are in keeping with published literature. Of interest is the high proportion of combined classes, which has not been described in other study populations.

The commonest presentation was of sub-nephrotic proteinuria. The association between proliferative LN classes and renal dysfunction is highlighted, emphasising the clinical importance of these classes in this population.

The HIV positive patient cohort (6%) showed possible histopathological and serological differences, however, due to the small number of cases, it was not possible to determine whether or not these differences were statistically significant.

1586 IgG/Albumin Staining Ratios in Protein Reabsorption Droplets in Renal Biopsies with Minimal Change Disease (MCD) and Focal Segmental Glomerulosclerosis (FSGS)

Lihong Bu[1], Mark Haas[2]
[1]University of Minnesota, Minneapolis, MN, [2]Cedars-Sinai Medical Center, Los Angeles, CA

Disclosures: Lihong Bu: None; Mark Haas: None

Background: Historically, selectivity of proteinuria for albumin was used to provide evidence for MCD in patients with nephrotic syndrome (NS), although this is rarely used today. However, in patients with NS, some renal biopsies cannot distinguish MCD from primary FSGS because of inadequate sampling and/or a lack of sampled glomeruli with segmental sclerosis in cases of early FSGS. For this reason, we examined whether staining of tubular epithelial protein reabsorption droplets for IgG and albumin, as a marker of selectivity of filtered protein, might help distinguish between MCD and FSGS.

Design: Frozen tissue from 145 native renal biopsies from patients with nephrotic range proteinuria, edema, and a diagnosis of MCD or FSGS (72 MCD, 31 FSGS-tip, 39 FSGS-NOS, 3 FSGS-collapsing), was retrospectively stained by direct immunofluorescence (IF) for IgG and albumin. Intensity of IgG and albumin staining of tubular protein reabsorption droplets was graded on a scale of 0 - 3+ by two observers for the first 45 cases and by one observer for the remaining 100, blinded to the diagnosis. Biopsies with FSGS lesions present on the frozen sections used for IF were excluded.

Results: Inter-observer agreement was 67% (30/45) for both IgG and albumin, with no disagreement >1+; IgG/albumin ratio agreement was 56% (25/45). Of the 72 MCD cases, 40 (56%) showed a ratio of 0 and only 9 (13%) a ratio >0.33; the mean ratio was 0.19 $\pm$ 0.24 (SD). By contrast, only 11/73 (15%) FSGS biopsies (9 FSGS-tip) had a ratio of 0. Fifty-three (73%) FSGS cases, including 15/31 FSGS-tip, 32/39 FSGS-NOS, and 3/3 FSGS-collapsing, had a ratio >0.33, with 16/39 FSGS-NOS cases having a ratio of 1 (Figure 1). The mean ratio was 0.60 $\pm$ 0.37 for all FSGS cases (P < 0.0001 vs MCD), 0.71 $\pm$ 0.30 for FSGS-NOS (P < 0.001 vs MCD and FSGS-tip), and 0.41 $\pm$ 0.33 for FSGS-tip (P = NS vs MCD). Of 85 biopsies with selective proteinuria (ratio $\leq$0.33), 63 (74%) had MCD, whereas among 20 with nonselective proteinuria (ratio $\geq$1.0), all but one were FSGS, including 16 FSGS-NOS (Figure 2).

Figure 1 - 1586

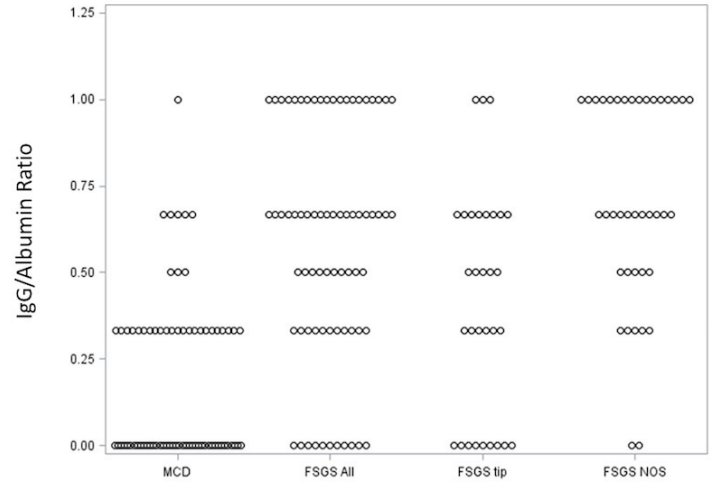

Figure 2 - 1586

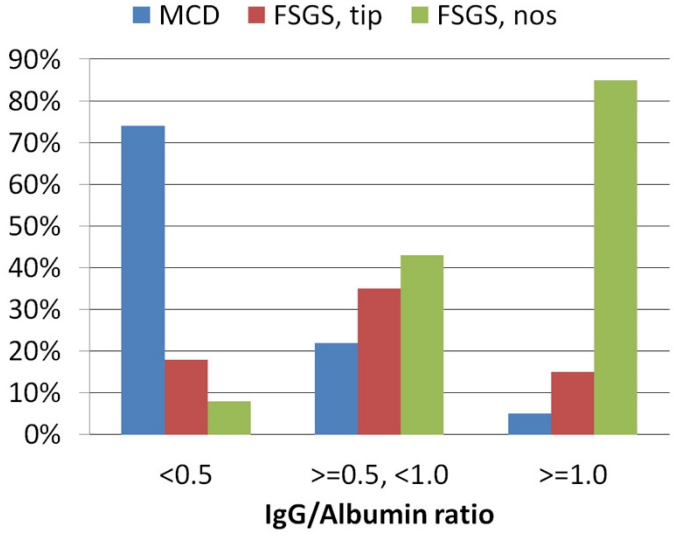

Conclusions: In this study of 145 renal biopsies from patients with MCD or FSGS, nephrotic range proteinuria, and edema, the IgG/albumin ratio in tubular epithelial protein reabsorption droplets was highly correlated with histologic diagnosis. A ratio of $\leq$0.33 was highly associated with MCD, while a ratio $\geq$1.0 was most often seen with FSGS-NOS.

1587 A Large Cohort of IgG4-Related Kidney Disease (IgG4-RKD)

Alessia Buglioni[1], Mariam Priya Alexander[1], Loren Herrera Hernandez[1], Mary Fidler[1], Samih Nasr[1], Sanjeev Sethi[1], Samar Said[2], Joseph Grande[1], Marie Hogan, Lynn Cornell[2]
[1]Mayo Clinic, Rochester, MN, [2]Rochester, MN

Disclosures: Alessia Buglioni: None; Mariam Priya Alexander: None; Loren Herrera Hernandez: None; Mary Fidler: None; Samih Nasr: None; Sanjeev Sethi: None; Samar Said: None; Joseph Grande: None; Marie Hogan: None; Lynn Cornell: None

Background: IgG4-related disease (IgG4-RD) is a systemic immune-mediated condition. Tubulointerstitial nephritis (TIN) is the most common renal involvement (IgG4-RKD); membranous glomerulonephritis (IgG4-MGN) is another recognized pattern.

Design: A biopsy (bx) and nephrectomy-based study from a single institution with clinicopathological correlation was performed in IgG4-RKD from 1/2001 to 9/2018.

Results: 102 patients (81 M, 21 F) were identified with IgG4-RKD on bx (n= 97) or nephrectomy for mass (n= 5). Samples showed TIN in 94% and/or MGN in 16%. Race/ethnicity among known patients was white (65%), African-American (11%), Asian (11%), Hispanic/Latino (11%), American Indian (3%). The mean age was 62 years (range 20-84). The primary indication for bx or nephrectomy was acute or chronic renal failure (71%), proteinuria (14%), and/or abnormal imaging/mass (22%). 55% had abnormal imaging, including masses (64%), enlargement (25%), and/or perinephric stranding (11%). Extrarenal involvement was present in 79%: 38% had one additional organ involved, 22% two, 19% three or more. Mean creatinine (SCr) at presentation was 3.2 mg/dl (median 2.4, range 0.7-11). For IgG4-MGN, the mean SCr was 2.2 mg/dl (range 0.7-6.6) and proteinuria was 7.3 g/d (range 1.2-16). Serum IgG4 was increased in 67% (n=28), C3 and/or C4 were decreased in 48%, and 28% had positive ANA.

TIN cases showed a plasma cell-rich infiltrate usually with expansile fibrosis. 92% showed increased IgG4+ plasma cells (focal >10 cells/40x field). (Diagnosis on other cases was established by the histologic pattern and other organ involvement by IgG4-RD.) None showed granulomatous inflammation. 70% showed tubular basement membrane immune complex deposits by IF or EM. Glomerular disease included MGN in 16 (92% PLA2R positive), IgA nephropathy in 2 (1 w/MGN), other immune complex GN in 4, and diabetic glomerulosclerosis in 8 (1 w/MGN).

Follow-up was available in 46 patients, with a mean of 21 months. 98% were treated with immunosuppression, including steroids in all, rituximab in 24%, and mycophenolate in 9%. 66% of patients with initially elevated SCr improved. 5 patients (10%) developed ESRD.

Conclusions: From a medical biopsy-based service, the most common manifestation of IgG4-RKD is TIN with functional impairment. MGN usually manifests as renal dysfunction with proteinuria. Hypocomplementemia is more common in IgG4-RKD compared to systemic IgG4-RD as reported in the literature. A significant minority have renal-limited disease.

1588 Maximizing Data Retrieval From Renal Biopsy Tissue Using Nonlinear Microscopy: Examining the Paraffin Block After Processing

Lucas Cahill[1], Milan Rosen[2], Tadayuki Yoshitake[3], Kyle Harrington[4], Preston Law[5], James G. Fujimoto[3], Seymour Rosen[6]
[1]MIT-Harvard, Cambridge, MA, [2]Newton, MA, [3]Massachusetts Institute of Technology, Cambridge, MA, [4]University of Idaho, Moscow, ID, [5]University at Buffalo, Amherst, NY, [6]Beth Israel Deaconess Medical Center, Boston, MA

Disclosures: Lucas Cahill: None; Milan Rosen: None; Tadayuki Yoshitake: None; Kyle Harrington: None; Preston Law: None; James G. Fujimoto: None; Seymour Rosen: None

Background: Nonlinear microscopy (NLM) enables evaluation of tissue similar to conventional optical microscopy of permanent sections, however, NLM does not require physical tissue sectioning. Instead, NLM visualizes multiple subsurface depths in a tissue specimen by scanning a short pulse laser and nonlinearly exciting fluorescence in a focused spot. Different depths can be imaged by adjusting the z axis of the microscope without having to physically section the tissue. Visualization of tissue in an H&E color scale is accomplished by rapid staining with nuclear and stroma\cytoplasmic fluorescent dyes.

Design: 10 renal biopsy paraffin blocks with 16 tissue fragments were deparaffinized, labelled with Hoechst and eosin, and optically cleared using benzyl alcohol benzyl benzoate. Two-dimensional cross-sectional images were acquired on an NLM microscope with a 20x water immersion objective through the entire tissue every 4 um in depth, effectively serial sectioning the biopsies. The NLM cross-sections were then reconstructed into 3D intact H&E-like models. The glomeruli were segmented and counted.

Results: NLM images closely resembled the appearance of permanent H&E sections. Imaging was possible up to several hundred microns in depth (the tissue varied from 88 to 660 µm) enabling rapid 3D imaging and evaluation without time-consuming sectioning. Furthermore, since physical sections were not required, serial imaging planes were intrinsically aligned with respect to each other and glomerular parameters such as the area profile could be quantitatively assessed (Fig. 1).

Surprisingly, the amount of tissue remaining in the block frequently exceeded the amount originally examined by paraffin sections and the annotated glomerular count in the residual tissue exceeded that examined in paraffin sections (Fig. 2). However, it is important to note that estimated glomerular count in renal biopsies generally is an underestimation (Rosenberg, Plos One, 2016). In NLM examined tissue, all glomeruli could be identified, examined and counted.

Figure 1 - 1588

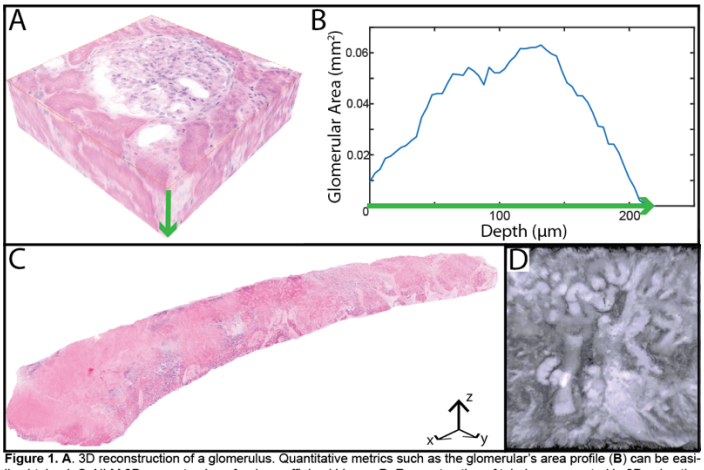

Figure 1. A. 3D reconstruction of a glomerulus. Quantitative metrics such as the glomerular's area profile (**B**) can be easily obtained. **C**. NLM 3D reconstrucion of a deparaffinized biopsy. **D**. Reconstruction of tubules segmented in 3D using the NLM volume.

Figure 2 - 1588

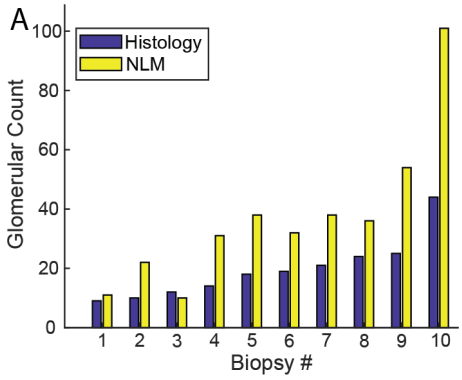

B

Biopsy #	Tissue thickness evaluated by NLM (μm)
1	660 and 232
2	448 and 268
3	264 and 332
4	292
5	368
6	200
7	368
8	388 and 88
9	380 and 216
10	392 and 472

Figure 2. A. Number of glomeruli counted on original biopsy histology slides vs. the number of glomeruli counted on the remaining tissue in the paraffin block using NLM. **B**. The thickness of the tissue fragments evaluated by NLM. Two numbers corresponds to two tissue fragments in that biopsy block.

Conclusions: These results indicate that the tissue in the paraffin blocks may be a valuable resource for future studies and that NLM may facilitate accurate quantitative analysis of complete tissue biopsies. One could speculate that this method may be utilized in initial renal biopsy processing to achieve a more complete tissue examination, since the usual paraffin processing is not altered in any way by this technique.

1589 APOL1 Expression Does Not Vary With Disease State in Patients with ApoL1 Risk Alleles

Tiffany Caza[1], Jon Wilson[2], Chris Larsen[2]
[1]Arkana Laboratories, Bryant, AR, [2]Arkana Laboratories, Little Rock, AR

Disclosures: Tiffany Caza: None; Jon Wilson: None; Chris Larsen: None

Background: Sequence variants of the *APOL1* gene contribute to an increased risk of non-diabetic nephropathy in African Americans. The pathogenic mechanisms by which these risk alleles result in disease are still being determined. Recent studies suggest environmental factors induce APOL1-associated nephropathy by increasing APOL1 transcripts in podocytes. We sought to investigate the degree of APOL1 expression in kidney biopsies with a histopathologic spectrum of APOL1-associated nephropathies and controls.

Design: DNA extracted from frozen renal biopsy tissue was genotyped for APOL1 G1 and G2 alleles using TaqMan Primer Probes. In patients with homozygosity or compound heterozygosity for APOL1 risk alleles (G1/G1, G1/G2, or G2/G2), *in situ* hybridization for APOL1 transcript using an RNAScope probe kit on a Leica BOND III platform was performed on FFPE tissue. ApoL1 mRNA counts were assessed by a ratio of signals to number of cells within podocytes of 5 intact glomeruli, 10 proximal tubules, and 10 distal tubules. UBC, PP1B, and bacterial gene DAPB were used for positive and negative controls. The specimens were grouped as controls without glomerulosclerosis (n=7), focal segmental glomerulosclerosis not otherwise specified (FSGS, n= 5), collapsing glomerulopathy (n=6), chronic kidney disease (CKD, n=5), membranous nephropathy (MG, n=6), and MG with collapsing lesions (n=7). ANOVA was performed to evaluate differences between groups.

Results: There were no significant differences in APOL1 expression within podocytes of intact glomeruli, proximal tubules, or distal tubules when comparing cases of FSGS, collapsing glomerulopathy, or CKD to controls ($p>0.05$ all groups). Although the glomeruli within areas of capillary tuft collapse did show increased ApoL1 expression, intact glomeruli within the same biopsies with collapsing glomerulopathy did not show the same increase. There were also no significant differences in tissue ApoL1expression when comparing MG with and without collapsing lesions to one another or controls ($p>0.05$ all groups, see table).

APOL1-associated nephropathy	Podocytes Mean APOL1 probe signals/cell ± SD	Proximal tubules Mean APOL1 probe signals/cell ± SD	Distal tubules Mean APOL1 probe signals/cell ± SD
Controls	3.18 ± 2.81	0.55 ± 0.17	0.99 ± 0.25
CKD / Arterionephrosclerosis	1.57 ± 1.08	0.47 ± 0.20	0.80 ± 0.21
FSGS	4.05 ± 1.76	0.61 ± 0.05	1.79 ± 0.60
Collapsing glomerulopathy	4.27 ± 2.68	0.76 ± 0.27	1.64 ± 0.85
MG	3.64 ± 1.40	0.69 ± 0.35	1.12 ± 0.53
MG with collapsing	2.25 ± 0.98	0.68 ± 0.18	1.11 ± 0.46

Conclusions: The clinicopathologic spectrum of APOL1-associated nephropathy ranges from chronic injury with slow decline in renal function to the most fulminant form, collapsing glomerulopathy that progresses to ESRD. The lack of difference in ApoL1 transcript expression between the histologic variants of APOL1-associated nephropathy and controls suggests that significant overexpression is not the primary driver of renal disease.

1590 Renal Manifestations of Common Variable Immunodeficiency

Tiffany Caza[1], IShin Wen[2], Chris Larsen[2]
[1]Arkana Laboratories, Bryant, AR, [2]Arkana Laboratories, Little Rock, AR

Disclosures: Tiffany Caza: None; IShin Wen: None; Chris Larsen: None

Background: Common variable immunodeficiency (CVID) is one of the most common primary immunodeficiency syndromes, yet is overall rare affecting 1/25,000-50,000 patients. To date, there are no case series of renal biopsies from CVID patients, making it difficult to determine whether individual case reports of renal disease in CVID represent sporadic events or are related to the underlying pathophysiology. Here, we present the first case series and review of the literature of nephropathology in CVID.

Design: A retrospective analysis of renal biopsy specimens in our database from patients with a clinical history of CVID was performed (n=18). Light, immunofluorescence, and electron microscopy were reviewed. For cases of membranous glomerulopathy, immunofluorescence for PLA2R and THSD7A were performed. Interstitial lymphoid infiltrates were phenotyped by CD3, CD4, CD8, and CD20 immunohistochemistry. A literature review was performed of all reported cases of native renal biopsies in CVID patients indexed on Pubmed, Scopus, or Google Scholar (n=24).

Results: Acute kidney injury and proteinuria were the leading indications for renal biopsy in CVID patients. Eight of 18 (44%) patients in our cohort and 8 of 24 (33%) of reported cases had immune complex glomerulonephritis with capillary loop immune deposits. Seven of 8 (87.5%) from our cohort had a membranous glomerulopathy and one case had membranoproliferative glomerulonephritis with IgG3 kappa deposits. All membranous glomerulopathy cases were PLA2R and THSD7A negative. IgG capillary loop deposits were present within all cases with variable expression of IgA, IgM, C3, and C1q. The second most common renal biopsy diagnosis was acute tubulointerstitial nephritis, affecting 6 of 18 (33%) in our cohort and 8 of 24 (33%) reported cases. All tubulointerstitial nephritis cases within our cohort showed tubulitis and a lymphocytic infiltrate that contained >90% $CD3^+$ T cells. Other renal biopsy diagnoses included acute tubular injury (n=1), AL amyloidosis (n=1), diabetic glomerulosclerosis (n=1), thin glomerular basement membranes (n=1), pauci-immune sclerosing glomerulonephritis (n=1), and arterionephrosclerosis (n=1). Reported in the literature, but not within our cohort was AA amyloidosis (n=8, 33% cases).

Conclusions: Membranous glomerulopathy and T-cell rich acute tubulointerstitial nephritis were the leading causes of nephropathology in CVID patients who underwent renal biopsy in our cohort and within the literature.

1591 KM55 is a Highly Specific but Insensitive Marker of IgA Nephropathy

Vivek Charu[1], Alejandro Best Rocha[2], Shree Sharma[3], Chris Larsen[3]
[1]Palo Alto, CA, [2]Little Rock, AR, [3]Arkana Laboratories, Little Rock, AR

Disclosures: Vivek Charu: None; Alejandro Best Rocha: None; Shree Sharma: None; Chris Larsen: None

Background: IgA nephropathy (IgAN) is a histopathologic diagnosis defined by glomerular deposition of IgA and is typically classified as "primary" or "secondary". Galactose-deficient IgA1 (Gd-IgA1) has been shown to be important in the pathogenesis of primary IgAN but its role in secondary IgAN remains unclear. We study the utility of KM55, a monoclonal antibody specific to Gd-IgA1, in determining the underlying etiology of IgAN.

Design: We retrospectively identified 75 cases of IgAN, 16 cases of lupus nephritis (LN), 11 cases Henoch-Schonlein Purpura nephritis (HSPN), and 3 cases non-immune complex mediated disease (NICMD) with at least three glomeruli on paraffin embedded sections to allow for immunohistochemical staining. Based on available clinical data at the time of biopsy, cases of IgAN were divided into the following

categories: probable primary IgAN (P-IgAN), probable secondary IgAN (S-IgAN), and infection-associated IgAN (IA-IgAN). Immunohistochemistry for KM55 was performed and the percentage of glomeruli with mesangial staining was calculated. All cases were scored in a blinded fashion by three renal pathologists.

Results: 75 cases of IgAN were further categorized as follows: 42 cases of P-IgAN, 14 cases of S-IgAN (10 with cirrhosis, 2 with inflammatory bowel disease, and 2 with psoriasis) and 19 cases of IA-IgAN. The mean/median percentages of glomeruli staining with KM55 was significantly different across the categories studied (p<0.0001, see Table). The majority of cases (86%) had less than 20% or more than 80% of glomeruli staining. Receiver operating characteristic (ROC) analysis using the percent of glomeruli staining with KM55 as a classifier demonstrates an area under the ROC curve of 84.0% (95% CI: 76.5 – 91.5%); a threshold of greater than 50.0% of glomeruli staining achieves a specificity of 100.0% and a sensitivity of 64.3% for identifying cases of P/S IgAN (v. IA-IgAN, LN, and NICMD).

	P-IgAN	S-IgAN	IA-IgAN	HSPN	LN	NICMD	p
Sample size (n)	42	14	19	11	16	3	
Age (median; IQR)	27.5 (22.0-36.7)	54.5 (47.3-62.5)	60.0 (57.5 -72.5)	7.0 (3.5-9.0)	27.0 (21.0-34.3)	53.0 (38.5-57.0)	< 0.001
Female (n; %)	18 (42.8)	3 (21.4)	3 (15.8)	5 (45.5)	11 (68.8)	1 (33.3)	0.02
No. of intact glomeruli by IHC (median; IQR)	12.0 (7.3-17.8)	8.0 (6.3-12.8)	12.0 (7.5-19.0)	25.0 (12.5-34.5)	13.5 (9.0-16.5)	16.0 (12.0-17.5)	0.7483
Percent of glomeruli staining for KM55 (%) (median; IQR)	81.7 (13.0-100.0)	86.1 (22.5-100.0)	0.0 (0.0-12.5)	16.0 (0-54.5)	0.0 (0.0-0.0)	0.0 (0.0-0.0)	
Percent of glomeruli staining for KM55 (%) (mean; range)	62.6 (0.0-100.0)	64.5 (0.0-100.0)	9.3 (0.0-44.4)	31.6 (0-100.0)	2.0 (0.0-16.7)	0.0 (0.0-0.0)	0.00145
No. with >50% glomerular staining (%)	27 (64.3)	9 (64.3)	0 (0.0)	3 (27.3)	0 (0.0)	0 (0.0)	<0.001

Table. Clinical characteristics and glomerular staining with KM55 for each of the subgroups studied. Abbreviations: P-IgAN: probable primary IgAN; S-IgAN: probable secondary IgAN; IA-IgAN: probable infection-associated IgAN; HSPN: probable Henoch-Schoenlein Purpura Nephritis; LN: lupus nephritis; NICMD: non-immune-complex-mediated disease.

Figure 1 - 1591

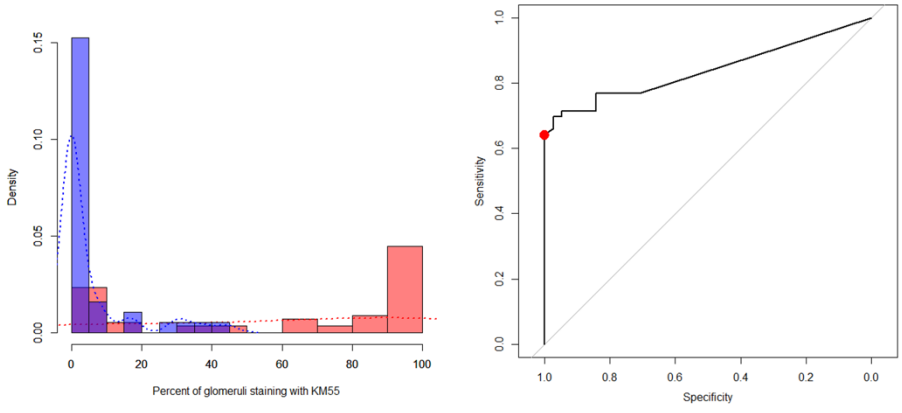

Figure. (Left panel) Histogram of P-IgAN and S-IgAN (red; n =56), compared with that of LN, IA-IgAN, and NICMD (blue; n = 38). (Right panel) Receiver operating characteristic (ROC) curve for KM55 glomerular staining in identifying P-IgAN and S-IgAN versus LN, IA-IgAN, and NICMD. The area under the ROC curve is 84.0% (95% CI: 76.5 – 91.5%). Considering a threshold of 50% of glomeruli staining with KM55 achieves a specificity of 1.0 and a sensitivity of 0.64 (red point). Abbreviations: P-IgAN: probable primary IgAN; S-IgAN: probable secondary IgAN; IA-IgAN: probable infection-associated IgAN; LN: lupus nephritis; NICMD: non-immune-complex-mediated disease.

Conclusions: KM55 is specific but insensitive marker of IgAN. Importantly, it may have utility as a marker to distinguish between P/S-IgAN and IA-IgAN, a commonly encountered diagnostic challenge. These data provide new insights into the pathogenesis of S-IgAN, in which Gd-IgA1 likely plays a significant role, and of IA-IgAN, in which glomerular IgA deposition likely occurs via a mechanism independent of Gd-IgA1 production. Among cases lacking KM55 staining, we cannot rule out the possibility of other epitopes of Gd-IgA1 that are unrecognized by KM55.

1592 Long-term Trends and Clinical Outcomes of Inpatient Percutaneous Renal Biopsies in the United States, 2001-2013

Vivek Charu[1], Michelle O'Shaughnessy[2], Glenn Chertow[2], Neeraja Kambham[3]
[1]Palo Alto, CA, [2]Stanford University School of Medicine, Palo Alto, CA, [3]Stanford University, Stanford, CA

Disclosures: Vivek Charu: None; Michelle O'Shaughnessy: None; Glenn Chertow: None; Neeraja Kambham: None

Background: Prior reports on bleeding complication rates associated with percutaneous renal biopsy (PRB) show significant variation and are based on low-volume single-center studies. Here we study long-term trends and clinical outcomes of inpatient PRBs in the US from 2001-13.

Design: The Nationwide Inpatient Sample is an ICD-coded ~20% sample of all US hospital discharges. We extracted discharges from 2001-13 with procedure codes for PRB and determined the frequency of packed red-blood cell (pRBC) transfusions as well as the relative timing between the PRB and transfusion. Outcomes considered were pRBC transfusion within 24 and 48 hours of PRB. We extracted data on several comorbidities: diabetes (DM), hypertensive disease (HD), chronic kidney disease (CKD), nephrotic syndrome (NS), acute renal failure (ARF), rapidly progressive glomerulonephritis (RPGN) and lupus. Trends in rates of PRBs were calculated using data from the US census. Logistic regression models were used to quantify risk factors associated with a pRBC transfusion within 48 hours of PRB.

Results: A total of 72,228 records with inpatient PRBs met our inclusion criteria. From 2001-13, native PRBs among all adults increased by 40% (from 8.0 to 11.0 per 100000 per year, $p<10^{-7}$), and transplant PRBs among adults aged 65 and older increased by 200% (from 1.0 to 3.0 per 100000 per year, p=0.0002). In contrast, annual rates of PRBs in the pediatric population were stable over the study period (0.7 and 2.4 per 100000 per year in transplant PRBs and native PRBs, respectively). Estimated rates of pRBC transfusions within 24 and 48 hours, respectively, are 3.0 and 5.0% among adult native PRBs, 2.9 and 4.4% among adult transplant PRBs, 1.5 and 2.2% among pediatric native PRBs, and 1.3 and 2.1% among pediatric transplant PRBs. Among adult native PRBs, adjusted analyses demonstrate statistically significant increased odds for pRBC transfusion within 48 hours associated with increasing age, ARF, RPGN and lupus (adjusted ORs range: 1.31-1.56); and decreased odds with NS, and PRBs occurring at urban teaching hospitals (aORs range: 0.67-0.84).

Figure 1 - 1592

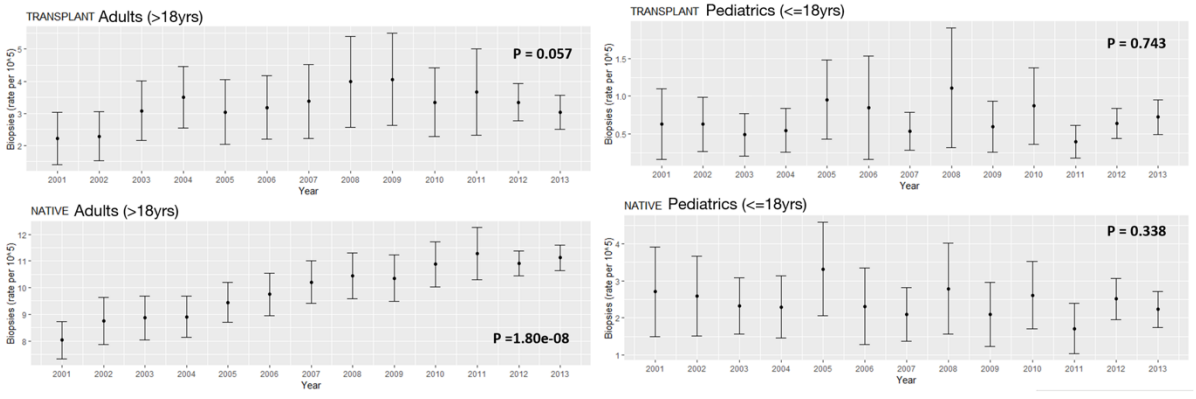

Figure. (Top left panel). Population-adjusted rates in percutaneous kidney biopsies (PRBs) among transplanted adults. (Bottom left panel). Population-adjusted rates in native PRBs among adults. (Top right panel). Population-adjusted rates in transplant PRBs in the pediatric population. (Bottom right panel). Population-adjusted rates in native PRBs in the pediatric population. Rates are provided as the number of PRBs per 100,000 population in the US per year. P-values reflect the statistical significance in trends over time (linear regression).

Conclusions: We report the largest study of inpatient PRBs and associated rates of post-biopsy pRBC transfusions. These data demonstrate substantial increases in the rates of adult native and transplant PRBs over the study period. Estimated rates of pRBC transfusion post-biopsy range between 1.3 and 5.0%, demonstrating that PRB is a safe procedure. Our estimates are not generalizable to the outpatient setting.

1593 Hemolysis-Associated Hemoglobin Cast Nephropathy: a Clinicopathologic Analysis of 26 Cases

Zeljko Dvanajscak[1], Chris Larsen[1], Christie Boils[1], Michael Kuperman[1], L. Nicholas Cossey[1], Nidia Messias[1], Patrick Walker[1]
[1]Arkana Laboratories, Little Rock, AR

Disclosures: Zeljko Dvanajscak: None; Chris Larsen: None; Christie Boils: None; Michael Kuperman: None; L. Nicholas Cossey: None; Nidia Messias: None; Patrick Walker: None

Background: Intravascular hemolysis and hemoglobinuria are known causes of acute renal injury. However, reports of renal injury due to hemoglobin casts are sparse in the literature and likely under-recognized. We sought to define the clinical features, kidney biopsy findings, and outcome of patients with Hemolysis-Associated Hemoglobin Cast Nephropathy (HAHCN).

Design: We conducted a retrospective analysis of 26 cases of HAHCN present in our database. We then collected and analyzed the presenting clinical and laboratory features, kidney biopsy findings, treatment, and outcome data.

Results: The mean patient age was 48 years (range 19-77) and the male-to-female ratio was 1:1. All patients presented with acute renal failure and the following representative mean laboratory values at the time of biopsy: creatinine 7.6 ± 0.6 (range 2.9-14.6) mg/dL, hemoglobin 8.2 ± 0.5 (range 2.0-12.5) g/dL, and lactate dehydrogenase 1479 ± 393 (range 250-3758) U/l. All biopsies showed acute tubular injury of varying degree and atypical pigmented casts with fine to coarse granularity and occasional rope-like morphology. The nature of the casts was confirmed using immunohistochemistry (IHC) for hemoglobin A. Interstitial fibrosis and tubular atrophy varied from none-mild. Etiologies were clinically determined in 21 cases (80.8%) and included DAT-positive autoimmune hemolytic anemia (8/21, 38.1%), drug-induced hemolytic anemia (5/21, 23.8%), procedure-related hemolysis (2/21, 9.5%), paroxysmal nocturnal hemoglobinuria (2/21, 9.5%), disseminated intravascular coagulation (2/21, 9.5%), transfusion of incompatible platelet units (1/21, 4.8%), and toxin ingestion (sodium nitrite) (1/21, 4.8%). Clinical intervention varied with hemodialysis (9/26, 34.6%), steroids and/or immunosuppressive regiments (9/26, 34.6%), plasmapheresis (4/26, 15.4%), and eculizumab (3/26, 11.5%). At follow-up (10.3 ± 2.2 [range 1-26] months), the mean serum creatinine was 1.4 ± 0.2 (range 0.6-3.7) mg/dL.

Conclusions: This study represents the first case series to detail the clinicopathologic parameters and outcomes of patients with HAHCN. Recognition of HAHCN on renal biopsy requires the presence of acute tubular injury with atypical casts positive for hemoglobin by IHC. In this series, despite the overall clinically severe acute kidney injury seen in HAHCN (requiring hemodialysis in 35%), renal function returned to baseline in the majority of patients, suggesting that HAHCN carries a favorable prognosis.

1594 Kidney Allograft Chronic Active Inflammation/Rejection: Analysis of Banff ti and i-IFTA Lesions in the Context of Contemporary Biopsies

Alton Farris[1], Carla Ellis[1], Thomas Rogers[2], Harold Sullivan[2], Howard Gebel[1], Robert Bray[1], Payaswini Vasanth[1]
[1]Emory University, Atlanta, GA, [2]Emory University/Medicine, Atlanta, GA

Disclosures: Alton Farris: *Consultant*, MedImmune, Inc.; Carla Ellis: None; Thomas Rogers: None; Harold Sullivan: None; Howard Gebel: None; Robert Bray: None; Payaswini Vasanth: None

Background: The Banff Conference for Allograft Pathology recently formally introduced diagnostic criteria for tubulointerstitial chronic active T-cell mediated rejection and scores for inflammation in areas of interstitial fibrosis and tubular atrophy (i-IFTA) and total inflammation (ti). This study sought to characterize our recent experience with these additions to the Banff Classification.

Design: Renal transplant biopsy reports at our center with i-IFTA and ti scores were retrieved, and rejection criteria and other clinicopathologic parameters pertaining to these biopsies were characterized.

Results: Renal transplant biopsy reports had available i-IFTA and ti scores for 263 biopsies since these scores were incorporated into our reporting in July 2017. Biopsies were performed at a median ± standard deviation (SD) of 228±94 days post-transplant. Mean creatinine ± SD was 4.0±2.8; and on linear regression, creatinine showed a weak correlation with i and ti scores (both $r = 0.21$, $p < 0.001$) but not the i-IFTA score. Acute T cell-mediated rejection (TCMR) was present at a grade of borderline (n=78), 1A (n=31), 1B (n=29), 2A (n=20), 2B (n=3), and 3 (n=4). Human leukocyte antigen (HLA) donor specific antibody (DSA) was detected as class I only (n=8), class II only (n=28), and class I and II (n=15); and antibody-mediated rejection could be diagnosed as active in 14 and chronic active in 19. A number of i, ti, and i-IFTA patterns were observed when tabulated and analyzed with hierarchical clustering (Figure), the most common of which had minimal or no inflammation (i0+ti0+i-IFTA0) (26%); and the next 3 most common patterns (accounting for 27%) had i≥2, ti≥2, and i-IFTA≥2. Based on the Banff t and ti scores, a diagnosis of chronic active TCMR in the tubulointerstitial compartment could be considered grade 1A in 37 and grade 1B in 44; and this was combined with acute TCMR in 68.

Figure 1 - 1594

i, ti, and i-IFTA Patterns:

	Pattern	#	%
1	i0+ti0+i-IFTA0	68	26%
2	i2+ti2+i-IFTA3	24	9%
3	i3+ti3+i-IFTA3	24	9%
4	i2+ti2+i-IFTA2	23	9%
5	i0+ti0+i-IFTA1	16	6%
6	i1+ti1+i-IFTA2	14	5%
7	i3+ti3+i-IFTA0	14	5%
8	i1+ti1+i-IFTA1	12	5%
9	i0+ti1+i-IFTA1	11	4%
10	i1+ti1+i-IFTA0	7	3%
	Others	50	19%

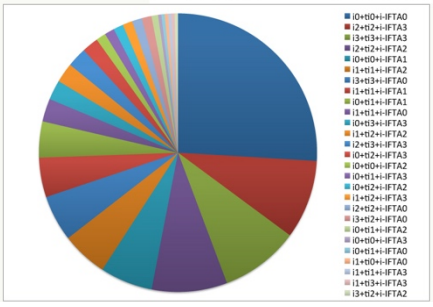

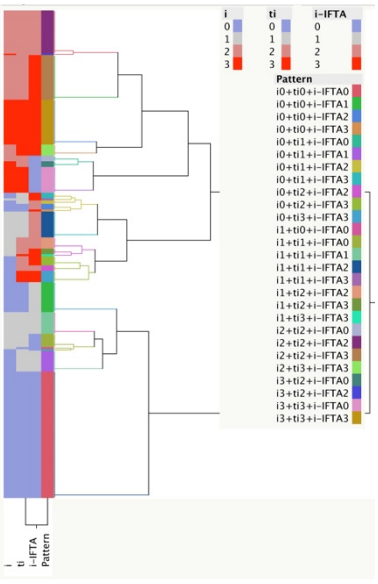

Conclusions: A variety of patterns can be seen with i, i-IFTA, and ti scores; and these are seen in a cohort with a mixture of T cell and antibody-mediated rejection. As specified in the recent Banff criteria for chronic active tubulointerstitial TCMR, which requires scores of ti≥2 and i-IFTA≥2, this cohort shows that i≥2 is accompanied by ti≥2 and i-IFTA≥2 in over a quarter of cases; therefore, a diagnosis of combined acute and chronic active TCMR can possibly be made in a noticeable subset of renal allograft biopsies. Larger studies are needed to explore the diagnostic, prognostic, and theranostic implications of these findings.

1595 Severe Arteritis in Kidney Allografts (Banff v2 to v3 arteritis): Clinicopathologic Correlations

Alton Farris[1], Carla Ellis[1], Thomas Rogers[2], Harold Sullivan[2], Howard Gebel[1], Robert Bray[1], Payaswini Vasanth[1]
[1]Emory University, Atlanta, GA, [2]Emory University/Medicine, Atlanta, GA

Disclosures: Alton Farris: *Grant or Research Support*, MedImmune, Inc.; Carla Ellis: None; Thomas Rogers: None; Harold Sullivan: None; Howard Gebel: None; Robert Bray: None; Payaswini Vasanth: None

Background: Arteritis is considered severe (v2 score) in the Banff Conference for Allograft Pathology system if it leads to a loss in at least 25% of the arterial luminal area, & v3 arteritis has transmural arteritis &/or fibrinoid change. It is recognized that severe (v2 to v3) arteritis can be a result of cellular &/or antibody-mediated rejection; however, full clinicopathologic characterization of cases with severe arteritis is still needed & was the aim of this study.

Design: Kidney allograft biopsies with v2 to v3 arteritis were retrieved during contemporary immunosuppression & human leukocyte antigen (HLA) donor specific antibody (DSA) testing at our center (2012–2015); & clinicopathologic features were assessed, including Luminex® single antigen bead DSA analysis.

Results: Criteria for v2 & v3 arteritis were fulfilled in 40 & 39 biopsies, respectively, representing 3.2% (79 of 2,436) of allograft kidney biopsies during the study period; & these rejection episodes occurred at a median±standard error (SE) of 235±126 days after transplantation. The patients were mostly (62%) male & had a mean±standard deviation age of 49±15 years. Creatinine peaked at mean±SE= 6.2±4.3 mg/dL (5.7±0.7 for v2 & 6.7±0.6 for v3, not significantly different by t-test). Simultaneous DSAs were detected in 25 patients (32%) (12 HLA class I&II, 3 class I only, & 10 class II only). DSAs were present in 7 of 48 patients on belatacept (15%) versus 18 of 31 not on belatacept (58%), a statistically significant difference (Chi-square p<0.0001). Dialysis return due to graft failure occurred in 10 v2 patients (25%) versus 21 v3 patients (54%), a statistically significant difference (Chi-square p=0.008). Banff criteria included mean±SE = t2.5±0.1, i2.4±0.1, g1.2±0.1, ptc1.2±0.1, cv0.9±0.1, ci1.1±0.1, ct1.1±0.1, cg0.3±0.1, & immunohistochemistry C4d0.7±0.1 [C4d0(negative)(n=52), C4d1(n=10), C4d2(n=6), & C4d3(n=11)].

Conclusions: Severe arteritis as assessed by this cohort (v2 to 3 arteritis) presented with marked renal functional impairment. As recognized previously, this confirms that v2 to v3 arteritis occurs without DSA, likely due to “pure” cellular rejection. In particular, prior v3 arteritis patients in the literature typically had more DSA. Immunosuppression apparently has a role, since DSAs occurred at a lower rate with belatacept. However, this still prompts consideration of other possible rejection mechanisms (e.g.,non-HLA antibodies); & larger arteritis cohorts may yield novel insights.

1596 Simple Collagen Imaging Camera (SCICam): a Novel Methodology for Collagen Detection and its Application to Renal Biopsies

Farzad Fereidouni[1], Eric Arauza[2], Austin Todd[1], Richard Levenson[3], Kuang-Yu Jen[1]
[1]University of California, Davis, Sacramento, CA, [2]University of California, Davis Medical Center, West Sacramento, CA, [3]UC Davis Health, Sacramento, CA

Disclosures: Farzad Fereidouni: None; Eric Arauza: None; Austin Todd: None; Richard Levenson: None; Kuang-Yu Jen: None

Background: The degree of interstitial fibrosis (ct, in the Banff system) is a key determinant of prognosis in kidney disease and is routinely reported as an estimation of total cortical involvement. Typically, a trichrome stain is performed to help highlight ct. However, even with such a stain, visual quantitation of ct is often subjective, imprecise, and suboptimal. Additionally, for some tasks such as assessing the suitability of deceased donor kidneys for use in transplantation, obtaining rapid and accurate ct estimation could be invaluable. Current routine practice in this setting is limited by frozen section artifact and the lack of rapid staining protocols for more sensitive special stains. We have developed a novel imaging methodology that we have termed SCICam, which provides a straightforward approach for highlighting collagen directly from H&E-stained slides, including frozen sections, without requiring additional sections or stains.

Design: SCICam takes advantage of spectral differences that distinguish different tissue components in order to segment or unmix specific collagen signals. It has whole-slide scanning capabilities for collagen detection and pixel-accurate alignment with conventional H&E-stained data. To test the reliability of SCICam, 50 formalin-fixed paraffin-embedded transplant renal biopsies representing a range of ct were imaged by SCICam using only H&E sections. The SCICam collagen signal was quantitated as a percentage of cortical involvement and each biopsy was categorized based on the Banff classification system for ct and compared to the original pathologist's reads.

Results: Overall, there was excellent correlation between ct Banff scores determined at original pathologist's reads and SCICam quantitation. The SCICam collagen signals were also mapped on the H&E section from which they were derived to produce pseudo-trichrome images that appear comparable to the corresponding trichrome slides from serial sections. (Figure 1).

Figure 1 - 1596

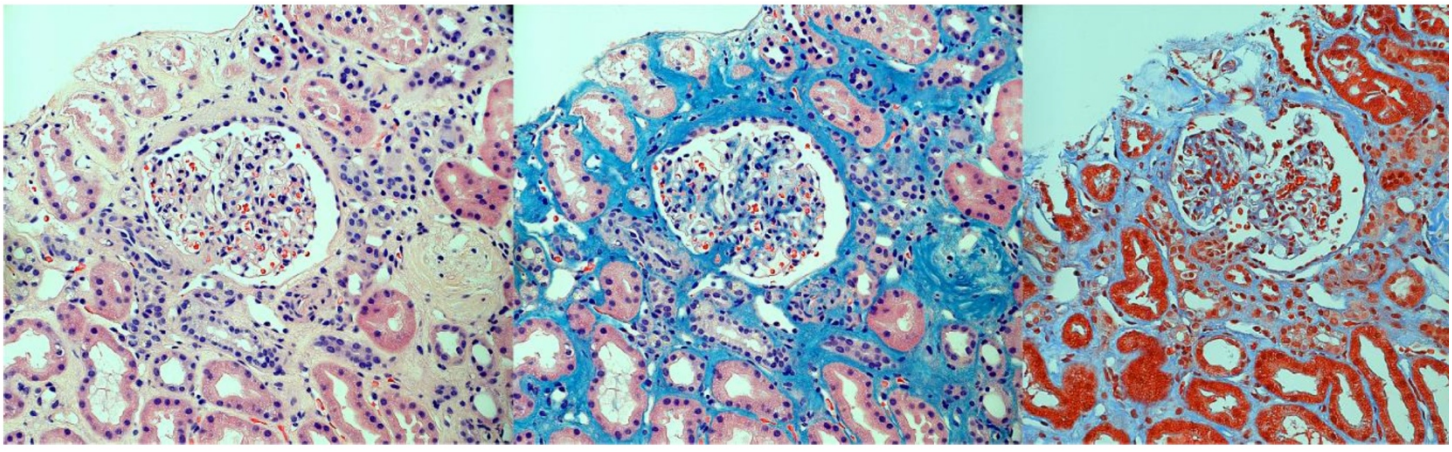

Figure 1: H&E *(left) and* SCICam *(middle)* image of the same field *with* collagen shown in Serial section *stained with* trichrome *(right).*

Conclusions: SCICam is a novel, simple, rapid, and inexpensive method to image collage from existing histologic slides. Its signal can be rapidly converted to create pseudo-trichrome stains to aid visual assessment of ct. It can also be subjected to automated computer scoring to improve precision. SCICam-based methods could be easily implemented into pathology workflow settings to improve turnaround and quantitative accuracy.

1597 Renal Vasculitis and Pauci-immune Glomerulonephritis in Patients Receiving Immune Checkpoint Inhibitor Therapy

Alexander Gallan[1], Ellen Alexander[2], Anthony Chang[3], Kammi Henriksen[3]
[1]Brookfield, IL, [2]The University of Chicago, Chicago, IL, [3]University of Chicago, Chicago, IL

Disclosures: Alexander Gallan: None; Ellen Alexander: None; Anthony Chang: None; Kammi Henriksen: None

Background: Immune checkpoint inhibitors (CPIs) have led to improved oncologic outcomes in a variety of solid organ and hematologic cancers. Monoclonal antibodies targeting programmed cell death 1 protein (PD-1), programmed death-ligand 1 (PD-L1), and cytotoxic T lymphocyte-associated antigen 4 (CTLA-4) block the inhibition of T cell activation by cancer cells, thereby potentiating the anti-tumor immune response. However, over-activation of the immune system can lead to immune-related adverse events (IRAEs). IRAEs are being increasingly reported in the kidney, with acute interstitial nephritis the most frequent pattern of injury. Biopsy-proven renal vasculitis or pauci-immune glomerulonephritis have only been described in a single case report, although vasculitis in other organs has been well-described.

Design: We identified 4 cases of renal vasculitis or pauci-immune glomerulonephritis in patients undergoing CPI therapy in the pathology archives from 2011 to 2018. Clinicopathologic features were reviewed.

Results: Clinicopathologic features of the 4 cases are detailed in Table 1. Three patients had renal small vessel vasculitis and one had focally crescentic pauci-immune glomerulonephritis. All patients were ANCA negative. The time from CPI initiation to IRAE presentation ranged from 2 weeks to 24 months. Patient 1 died from a myocardial infarction. Patient 4 received pulse steroids with resolution of AKI. Patients 2 and 3 received high-dose steroids, but limited clinical followup was available.

Case	Age/Sex	History	CPI	Presentation	# Months After CPI Initiation	Pathology
1	68/M	Mucosal melanoma	Nivolumab	AKI (SCr = 1.7), arthralgias, leukocytosis	<1	[Autopsy] Renal vasculitis, lymphocytic hypophysitis, pulmonary vasculitis
2	71/F	Lung adenoCa	Pembrolizumab	Purpuric rash, nephrotic syndrome, hematuria	10	Focally crescentic pauci-immune glomerulonephritis
3	75/F	Non-small cell lung Ca	Nivolumab	AKI (SCr = 6.1)	24	Renal vasculitis and granulomatous interstitial nephritis
4	63/F	Choroidal melanoma	Nivolumab	AKI (SCr = 5.5)	3	Renal vasculitis, interstitial hemorrhage, and interstitial nephritis

Conclusions: Our study demonstrates that renal vasculitis and pauci-immune glomerulonephritis are occasionally observed in patients receiving CPI therapy, adding to the spectrum of CPI-related IRAEs. The temporal relationship between the initiation of CPI therapy and kidney injury was variable, ranging from 2 weeks to 24 months. With increasing utilization of CPIs, renal pathologists and nephrologists should be aware of this association.

1598 HLA-DQ Donor Specific Antibodies Significantly Correlate with Interstitial Inflammation (i) and Tubulitis (t) Banff Scores in Kidney Allografts with Antibody Mediated Rejection

Cynthia Harris[1], Lisa Anderson[2], Ron Shapiro[3], Veronica Delaney[2], Stephen Ward[2], Madhav Menon[2], Fadi Salem[2]
[1]Massachusetts General Hospital, Boston, MA, [2]Icahn School of Medicine at Mount Sinai, New York, NY, [3]Recanati/Miller Transplantation Institute, New York, NY

Disclosures: Cynthia Harris: None; Lisa Anderson: None; Ron Shapiro: None; Veronica Delaney: None; Stephen Ward: None; Madhav Menon: None; Fadi Salem: None

Background: Borderline rejection (BR) and T-cell mediated rejection (TCMR) often co-occur with antibody-mediated rejection (AMR). We examined the association between interstitial inflammation in patients with histologic features of AMR and mean fluorescence intensity (MFI) of donor specific antibodies (DSA), specifically HLA-DQ.

Design: Renal biopsies with histopathology features consistent with AMR according to Banff were retrieved from the archives of our institution's Department of Pathology over a 6 year period. Demographic and clinical data, including results of DSA testing, were obtained by retrospective chart review. The cohort was restricted to patients who had DSA testing performed within 30 days of their biopsy. We analyzed the impact of interstitial inflammation and tubulitis and (i and t) co-existing with histopathologic evidence of AMR on the presence of DSA against Class I and Class II HLA, specifically HLA-DQ, and DSA MFI.

Results: We identified 119 unique patients whose biopsies showed histopathology consistent with AMR and who had DSA testing performed within 30 days of their biopsy. DSA results were positive (>1,000 MFI) in 75 patients (63.0%) [42 Class I, 66 Class II, 33 Class I and II].

Comparing associations of individual DSAs with i and t scores, HLA-DQ had a strong positive correlation with i score (r=0.43), t score (r=.292), and i+t score (r=0.40) (p<0.01 for all). Mean i scores increased with increasing DQ MFI (<1000, 1000-10000, >10000 – 0.8, 1.6, 2.0; ANOVA p<0.0001). A similar relationship was seen with i+t scores (<1000, 1000-10000, >10000 – 1.6, 3.0, 3.5; ANOVA p<0.0001). Interestingly, anti-HLA-A, B, and DR DSAs did not show any significant association with i or t scores by spearman correlation or ANOVA.

Fifty-six of 19 (47.1%) were explicitly diagnosed by the reviewing pathologist as having TCMR, of which 40/56 had positive DSA. Presence of TCMR and AMR was associated with a significantly increased odds of having DQ DSA (OR=4.19 and 3.78 DQ vs. DR and DQ vs. any Class I DSA comparisons, respectively; p<0.05).

Conclusions: Banff scores for tubulitis (t) and interstitial inflammation (i) in patients with co-existing histopathologic evidence of AMR are significantly correlated with HLA-DQ status. This finding raises questions pertinent to the pathogenesis of mixed rejection.

1599 Utility of Sox 9 immunohistochemistry in the Identification of Acute Tubular Injury in Kidney Biopsies

David Henriquez Ticas[1], Luan Truong[2], Liye Suo[1], Sadhna Dhingra[1]
[1]Baylor College of Medicine, Houston, TX, [2]Houston Methodist Hospital, Houston, TX

Disclosures: David Henriquez Ticas: None; Luan Truong: None; Liye Suo: None; Sadhna Dhingra: None

Background: Acute tubular epithelial injury (ATN) clinically manifests as rising in serum creatinine. Correlation of increased serum creatinine and ATN morphology in renal biopsies is not consistent. Sox 9 is a member of the Sry-related transcription factors, which is expressed in kidneys during nephrogenesis. Animal studies have shown upregulation of Sox9 in acute tubular epithelial injury. We studied the immunohistochemical expression of Sox9 for assessment of acute tubuloepithelial injury in renal biopsies.

Design: We identified 14 cases of renal biopsies, 7 allografts and 7 natives, using text search “kidney” and “acute tubular injury” for this study. For comparison, we selected 14 cases of renal biopsies, 9 allografts and 5 natives that did not show morphologic evidence of acute tubular injury on hematoxylin and eosin stain. Immunohistochemical stains for Sox9 and MIB-1 were performed on formalin-fixed, paraffin embedded tissues. A semiquantitative scoring was performed about the % of renal cortex positive for tubular nuclear staining: score 0: no staining; score 1: 25%; score 2: 26% to 50%; score 3: 51% to 100%. Immunostain for MIB 1 was evaluated for % of tubular nuclei staining in hot spots.

Results: In kidney biopsies with morphological evidence of acute tubular injury, 10/14 (71%) cases showed score 3 for Sox 9 immunostaining. The expression was diffuse and strong nuclear in proximal tubules with a relatively weaker expression in distal tubules. No case (0%) showed score 0 (no staining) in this group. Some cases showed concomitant cytoplasmic staining and focal staining of the brush borders. All cases in this group showed MIB 1 expression. It ranged from 4% to 10% in hotspots in 7/14 (50%) cases. In kidney biopsies with no morphological evidence of acute tubular injury, 2/14 (14%) cases were completely negative (score 0) for Sox 9 expression. The negative cases showed cytoplasmic staining and staining of the retained brush borders. Only 4/14 (28%) cases showed diffuse and strong nuclear Sox9 expression (score 3). Remaining 8 cases (57%) showed variable staining with a score of 1-2. For MIB 1, two cases (14%) were negative and remaining 12/14 (85%) cases shows variable MIB 1 with 1% to 5% positivity in hot spots.

Conclusions: Nuclear expression of Sox9 is increased during acute tubular injury. It can be used as a supportive tool for kidney biopsy interpretation in clinically suspected cases of acute tubular injury. MIB-1 showed evidence of tubular regeneration.

1600 Epigallocatechin-3-gallate inhibits renal light chain amyloidogenesis by two different mechanisms

Guillermo Herrera[1], Elba Turbat-Herrera[1], Jiamin Teng[2], Chun Zeng[2], Luis Del Pozo Yauner[2]
[1]University of South Alabama, Mobile, AL, [2]LSU Health Sciences Center, Shreveport, LA

Disclosures: Guillermo Herrera: Non; Jiamin Teng: Non; Chun Zeng: Non; Luis Del Pozo Yauner: None

Background: Previous reports have shown that epigallocatechin-3-gallate (EGC3G) can inhibit the amyloid aggregation of the light chains (LC) by direct interaction with the protein. Also, we have shown that treatment of mesangial cells (MCs) with amyloidogenic LC results in internalization of the protein by a receptor-mediated mechanism and the subsequent aggregation of the protein into fibrils in the lysosomal compartment. This process is tightly linked to transformation of MC into macrophage-like phenotype. In this study we show that EGC3G can inhibit light chain amyloidogenesis by stabilizing a non-amyloidogenic conformation of the LC and by inhibiting a mesangial cell signaling pathway linked to both phenotypic transformation and intracellular amyloid formation in lysosomas.

Design: Inhibitory activity of EGC3G was determined in a thioflavin-based fibrillogenesis assay with the lambda-6 light chain variable domain protein 6aJL2. Conformational changes of 6aJL2 caused by interaction with EGC3G were evaluated in dot-blot assays with a set of five different rabbit polyclonal antibodies that recognize non-native conformers of the protein. The inhibitory activity of EGC3G on the amyloidogenesis of LC in MCs was performed in cell culture, ex-vivo kidney model with perfusion of the LC through the renal artery.

Results: EGC3G inhibited in a concentration dependent manner the *in vitro* fibrillogenesis of the lambda-6 protein 6aJL2. The pattern of antibody recognition of the protein during the fibrillogenesis in presence of EGC3G is consistent with the accumulation of a non-native conformer that appears to be off-pathway of amyloidogenesis. After incubation with AL-LC and ex-vivo kidney experiment, fibrillar aggregates were observed in mesangial areas and c-fos was translocated into nuclei. In EGC3G treated group, cytoplasmic to nuclear translocation of c-fos was inhibited and intracellular amyloid fibril formation significantly decreased.

Conclusions: ECG3G can inhibit the amyloid aggregation of light chain in kidney by two different mechanism. One of them is the stabilization of the amyloid precursor in a conformer not apt to aggregate into fibrils. The second depends on the inhibition of the cytoplasm-to-nuclei translocation of c-fos in MCs.

1601 DNAJB9 IHC in the Diagnosis of Fibrillary Glomerulonephritis

Wesley Hiser[1], Agnes Fogo[1]
[1]*Vanderbilt University Medical Center, Nashville, TN*

Disclosures: Wesley Hiser: None; Agnes Fogo: None

Background: Fibrillary glomerulonephritis (FGN) is a rare disease, comprising up to 1% of native renal biopsies, and has classically been characterized by polyclonal IgG staining and the presence of Congo red negative, randomly oriented 12-22 nm fibrils. While these features are typical of FGN, there remains significant morphologic overlap with other glomerular diseases. DnaJ heat shock protein family(Hsp40) member B9 (DNAJB9) expression was recently reported to show consistent overexpression in cases of FGN when compared with other, morphologically similar glomerular diseases such as amyloidosis. In this study, we aimed to further investigate the sensitivity and specificity of IHC for DNAJB9 in the diagnosis of FGN.

Design: Renal biopsy specimens meeting standard diagnostic criteria for FGN with glomeruli available for IHC were identified from the past five years. IHC for DNAJB9 was performed on renal biopsies from 47 patients, two of which had repeat biopsies, with 39 cases diagnosed as FGN and ten consistent with FGN. IHC was also performed on 21 amyloidosis biopsies; 18 AL, two AA, and one indeterminate type. Glomerular staining was considered to be positive regardless of extent or intensity.

Results: 43 cases of FGN were DNAJB9 positive with smudgy to granular glomerular staining, eight of which had weak, variable staining patterns, with polyclonal IgG in 36 cases, monoclonal IgG in four, and monoclonal IgM in three. There was focal granular to pseudolinear staining of tubular basement membranes in 12 cases and of peritubular capillaries in an additional six. The average fibril diameter was around 18 nm. Six cases did not stain with DNAJB9, with polyclonal IgG staining in two of these cases, polyclonal IgM in one, kappa-predominant IgG1 in two, and C3 dominant staining in one. The average fibril diameter in these cases was around 15 nm. All cases of amyloidosis were DNAJB9 negative, giving IHC for DNAJB9 a sensitivity of 88% and specificity of 100% for FGN.

Conclusions: DNAJB9 IHC is a sensitive and specific marker for FGN, with strong staining in the majority of cases. While extraglomerular staining was only present with glomerular staining, DNAJB9 positive and negative cases of FGN showed similar incidence of clonality and fibril size. Some DNAJB9 negative cases exhibited atypical features by traditional diagnostic modalities, such as membranous pattern, C3 dominance, and IgM dominance with C1q. We conclude DNAJB9 IHC is a useful addition to current diagnostic criteria in the diagnosis of FGN.

1602 Deep Learning Based Detection of Normal and Globally Sclerotic Glomeruli on Whole Slide Images from the NEPTUNE Renal Biopsies with HE, PAS, Trichrome and Silver Staining

Catherine Jayapandian[1], Yijiang Chen[2], Andrew Janowczyk[1], Mathew Palmer[3], John O'Toole[4], John Sedor[4], Laura Barisoni[5], Anant Madabhushi[1]
[1]*Case Western Reserve University, Cleveland, OH,* [2]*Case Western Reserve University, Cleveland Heights, OH,* [3]*University of Pennsylvania, Philadelphia, PA,* [4]*Cleveland Clinic, Cleveland, OH,* [5]*University of Miami, Miami, FL*

Disclosures: Catherine Jayapandian: None; Yijiang Chen: None; Mathew Palmer: None; John O'Toole: None; John Sedor: None; Laura Barisoni: None; Anant Madabhushi: None

Background: Clinically useful quantitative assessment of renal biopsies requires robust methodologies to quantify normal and abnormal tissue structures. For example, the accurate estimate of percentage of globally sclerotic glomeruli adjusted for age can predict outcome, as we have demonstrated that accurate estimates of glomerular global sclerosis (GS) adjusted for age can predict outcomes across proteinuric diseases. However, visual assessment is poorly reproducible and time consuming. To increase efficiency, we present a deep

learning-based approach for computational detection and segmentation (object extraction) of normal and globally sclerotic glomeruli (histologic primitives) on digital images of renal biopsies with HE, PAS, Trichrome(TRI) and Silver(SIL) stains.

Design: We used 146, 105, 92, and 100 cropped images from 580 whole slide images (WSI) from 129 NEPTUNE renal biopsies of patients with Minimal Change Disease with (32) and without (97) global sclerosis, stained with PAS, TRI, SIL and HE. Convolutional neural network (CNN) architecture based on Alexnext was trained using transfer learning to produce 3 classifiers: (i) normal glomerular tuft, (ii) normal glomerulus (tuft + Bowman's capsule), and (iii) GS. The WSIs were divided into training and testing sets at the patient level with a ratio of 8:2.

Results: The detection and pixel level segmentation results for all 6 classifiers was graded via the F-score (A measure of classification accuracy that considers both precision and recall; 1 = perfect, 0 = worst) The classifiers were able to detect almost all glomeruli in the test images. Detection of normal glomeruli was more accurate than glomerular tuft and GS, with accuracy being greater from Trichrome > Silver > PAS > HE.

Model	Magnification	Segmentation F-scpre
Normal glomerular tuft – HE stain	5X	0.808
Normal glomerulus – HE stain	5X	0.844
Global glomerulosclerosis – HE stain	8X	0.644
Normal glomerulus – trichrome stain	5X	0.906
Normal glomerulus – PAS stain	5X	0.825
Normal glomerulus – Silver stain	5X	0.896

Conclusions: The development of these 6 CNNs represents the first step in evaluating renal biopsies using novel machine-human interactive protocols. The next step works include using these segmentation results for computer-aided diagnosis, validating the results on multi-institutional data and adding in more cases with a variety of kidney conditions.

1603 A Proposal for Pathologic Criteria to Diagnose Lupus Nephritis

Satoru Kudose[1], Dominick Santoriello[2], Andrew Bomback[3], Michael Stokes[4], Vivette D'Agati[5], Glen Markowitz[6]
[1]New York, NY, [2]New York-Presbyterian/Columbia University Medical Center, New York, NY, [3]Columbia University, New York, NY, [4]Columbia University College of Physicians and Surgeons, New York, NY, [5]Tenafly, NJ, [6]Columbia Presbyterian Medical Center, Tarrytown, NY

Disclosures: Satoru Kudose: None; Dominick Santoriello: None; Andrew Bomback: None; Michael Stokes: None; Vivette D'Agati: None; Glen Markowitz: None

Background: In 2012, the Systemic Lupus International Collaborating Clinics (SLICC) proposed that lupus nephritis (based on ISN/RPS classification), in the presence of positive ANA or anti-dsDNA antibody, is sufficient to diagnose SLE. However, this "stand-alone" renal biopsy criteria is problematic, because the ISN/RPS classification does not specifically define lupus nephritis (LN). We sought to identify the pathologic criteria which are most characteristic of LN.

Design: Three hundred consecutive biopsies with LN and 560 contemporaneous biopsies with non-lupus immune complex glomerulonephritis (ICGN) were reviewed. LN was diagnosed if: (1) there was a clinical diagnosis of SLE and (2) renal biopsy revealed ICGN consistent with LN. The control group consisted of consecutives biopsies showing IgA nephropathy (n=100), membranous glomerulopathy (100), pauci-immune glomerulonephritis (GN) (100), membranoproliferative GN (excluding C3 GN; 77), infection-related GN (47), ICGN not otherwise specified (36), and 25 cases each of anti-GBM disease, proliferative GN with monoclonal immunoglobulin deposits (PGNMID), fibrillary GN, and C1q nephropathy.

Pathology reports were reviewed for the following features that are characteristic of LN: dominant or co-dominant immunofluorescence (IF) staining for IgG, ?2+ intensity IF staining for C1q (scale 0-3+), "full-house" IF staining (IgG, IgM, IgA, C3, *and* C1q), IF or electron microscopic (EM) evidence of extra-glomerular deposits, presence of subendothelial, mesangial, and subepithelial deposits by IF or EM, and endothelial tubuloreticular inclusions. Receiver-operating characteristics curves were compared using DeLong's method.

Results: Table 1 provides the sensitivity and specificity of 5 individual pathologic features, and combinations thereof, for the diagnosis of LN. The presence of at least two of the five features had a sensitivity of 92% and specificity of 89%, while three or more of the five features had a sensitivity of 80% and specificity of 95%. These two thresholds were statistically equivalent (p>0.05).

Table 1. Sensitivity & Specificity of Pathologic Features and Proposed Criteria for Diagnosis of LN					
Features	**Full-house staining***	**?2+ intensity staining for C1q**	**Subendothelial & subepithelial deposits**	**Extra-glomerular deposits**	**Endothelial Tubuloreticular inclusions**
Sensitivity	71%	68%	75%	79%	80%
Specificity	90%	88%	80%	93%	96%
Number of Features Present**	**?1 of 5**	**?2 of 5**	**?3 of 5**	**?4 of 5**	**All 5**
Sensitivity	98%	92%	80%	66%	37%
Specificity	65%	89%	95%	98%	99%
***defined as ? +/- intensity staining for IgG, IgA, IgM, C1q and C3 on a scale of 0 to 3 **5 features considered: 1) Full house staining; 2) ≥2+ intensity staining for C1q; 3) Subendothelial & subepithelial deposits; 4) Extra-glomerular deposits; 5) Endothelial tubuloreticular inclusions.**					

Conclusions: The presence of ?2 of 5 characteristic pathologic features, in the presence of a positive ANA or anti-dsDNA antibody, reliably distinguishes most cases of LN from non-lupus ICGN. We propose that these features may form the basis for defining the SLICC "stand alone" LN criterion for the diagnosis of SLE.

1604 Glomerular Endothelial Injury Can Be Identified by Myeloperoxidase Immuno-Staining in Various Renal Disorders Related to Complement Activation

Tripti Kumar[1], Anthony Chang[2], Ping Zhang[3]
[1]Royal Oak, MI, [2]University of Chicago, Chicago, IL, [3]William Beaumont Hospital, Birmingham, MI

Disclosures: Tripti Kumar: None; Anthony Chang: *Speaker*, Alexion; Ping Zhang: None

Background: Multiple in vitro and in vivo studies report that complement can be activated by circulating myeloperoxidase (MPO) during their interactions with endothelial cells. MPO can be further taken up by endothelial cells. Then MPO generated hypochlorite and/or its associated 3-nitrotyrosine may cause additional endothelial injury. As complement activation is associated with various renal diseases, this study investigated whether MPO immuno-staining can be helpful in identifying glomerular endothelial injury in variants of renal diseases that are more or less related to complement activation.

Design: The study included normal kidney tissue as controls (n = 12), ANCA associated crescentic glomerulonephritis (CGN, n = 19), C3 dominant glomerulopathy (C3GN, n = 23), and thrombotic microangiopathy (TMA n = 21). All sections were stained for MPO by immunohistochemical method (Ventana pre-diluted rabbit polyclonal myeloperoxidase antibody). The cytoplasmic MPO staining in glomerular endothelial cells was semiquantitatively scored (0 to 3+).

Results: MPO was entirely negative in glomerular endothelial cells of all negative controls (0/12). In the CGN group, MPO stained positively (1 to 2 +) in endothelial cells of glomerular capillaries in 16/19 cases (84%), involving 20% to 100% of glomeruli in each case while the positive MPO staining in endothelial cells was parallel with crescent formation. MPO positive staining was seen in 61 % (14/23) of C3GN, while 38% (8/21) of cases with TMA showed positive glomerular endothelial staining for MPO.

Figure 1 - 1604

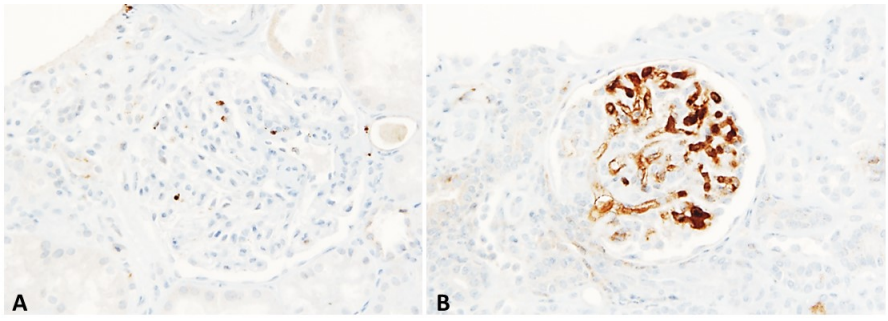

Negative control MPO 3+ staining

Conclusions: Our observation of positive MPO endothelial staining in a variety of renal diseases but not in controls supports that MPO can be upregulated by glomerular endothelial cells in human renal diseases. In addition, our data suggest that MPO immuno-staining may be used as a marker to highlight glomerular endothelial injury in renal diseases that are potentially related to complement activation.

1605 High Kidney Injury Moelcule-1 (KIM-1) Staining /Serum Creatinine (sCr) Ratio Is Associated with Better Renal Functional Recovery After Acute Tubule Injury in Native Kidneys

Tripti Kumar[1], Wei Li[2], Hassan Kanaan, Ping Zhang[3]
[1]Royal Oak, MI, [2]Beaumont Health, Royal Oak, MI, [3]William Beaumont Hospital, Birmingham, MI

Disclosures: Tripti Kumar: None; Wei Li: None; Hassan Kanaan: None; Ping Zhang: None

Background: Kidney injury molecule-1 (KIM-1) is a specific injury marker of proximal tubules. We have reported that higher KIM-1/sCr (K/C) ratio is associated with better recovery of transplant renal function, possibly due to K/C ratio reflecting an acute injury in intact proximal tubules (Kidney International 2008). The purpose of this study was to determine whether higher K/C ratio correlated with better improvement in renal dysfunction of native kidneys.

Design: In the first cohort, 11 controls with normal sCr and 37 indicated native biopsies with acute tubular injury were randomly selected for KIM-1 staining (AKG7 monoclonal antibody from JV Bonventre's lab, BWH, graded 0 to 3+ in proximal tubules), PAS evaluation for brush borders (scored 0 to 3+), and sCr follow-up over 6 months. In the second cohort, we randomly selected 184 renal biopsies from children to elders with acute renal diseases. Pediatric group had age < 20 years old (G1), while adults patients were also divided into non-senior group (G2, < 65 yr) and senior group (G3, >65 yr). KIM-1 staining and sCr levels were evaluated in all three groups.

Results: In the first cohort, KIM-1 and PAS were both significantly correlated with sCr levels ($p < 0.05$). PAS/sCr ratio (0.56 ± 0.06) and K/C ratio (0.57 ± 0.06) were also both significantly related to better reductions in sCr over 6 months. In the second cohort, positive staining of KIM-1 was seen in the majority of biopsies (80% to 91% in all groups), while the KIM-1 staining scores were significantly associated with high levels of sCr. Compared to adult renal biopsies (0.65 ± 0.09 in G2 and 0.55 ± 0.06 in G3), there was a higher KIM-1/sCr ratio (1.27 ± 0.13 in G1) in pediatric cases.

Conclusions: Our data indicate that K/C ratio was associated with better native renal functional recovery as PAS/sCr ratio does. Pediatric K/C ratio was higher than adults' ones. A high KIM-1/sCr ratio could be a potential repair and regeneration predictor in the early phase of AKI, accelerating the recovery of renal function after injury.

1606 Deep Learning Approach for Detecting, Localizing, and Typing Electron-dense Deposits in Renal Biopsies

Nasma Majeed[1], Alaa Alsadi[1], Charisse Liz Baste[1], Lucy Fu[2], Yash Dharmamer[1], Uwadia Edomwonyi[1], Dereen Mohammed Saeed[1], Suman Setty[3], Manmeet Singh[4], Tushar Patel[1]
[1]University of Illinois at Chicago, Chicago, IL, [2]Northwestern University Feinberg School of Medicine, Chicago, IL, [3]University of Illinois at Chicago Hospital and Medical Center, Chicago, IL, [4]Burr Ridge, IL

Disclosures: Nasma Majeed: None; Alaa Alsadi: *Major Shareholder*, Diagnosis Protocol; Charisse Liz Baste: None; Lucy Fu: None; Yash Dharmamer: None; Uwadia Edomwonyi: None; Dereen Mohammed Saeed: None; Suman Setty: None; Manmeet Singh: None; Tushar Patel: None

Background: Accurate diagnosis based on renal biopsy specimens require correlation between light microscopy, immunofluorescence, and electron microscopy studies. In cases where immune-mediated processes are suspected, identifying and distinguishing electron-dense deposits that are morphologically consistent with immune-complexes is a difficult, time-consuming, and consequently variable task. We explore deep learning (DL) approaches to facilitating this process by presenting them with screened images localizing potential regions of interest (ROI) that harbor the deposits, identifying and suggesting the predominant location of deposits (e.g. subendothelial vs subepithelial vs mesangial etc.), and further characterizing the deposit composition.

Lack of deep learning initiatives in renal pathology (especially compared with radiology and other areas of pathology) could be attributed to the perceived complexity of deep learning. We leveraged publically available, graphical user interfaces (GUI) based deep learning platforms to develop an approach for achieving the above potentials with mainly departmental resources.

Design: We identified more than 30,000 ".tif" EM images for cases between 2003 and 2018. Natural language queries to assemble prototyping data samples of Lupus Nephritis (contains deposits) and Negative-for-deposits are used to extract images. We designed a DL workflow to be independent from extra-departmental resources (namely engineering/ Computer science human capital). Images were deidentified, sorted and labeled with image data set management tools (Diagnosis Protocol), uploaded to cloud-based commercial DL platforms (Customvision.ai from Microsoft and AutoMLvision from Google) as well as to server-based expert platforms (DIGITS from NVIDIA) for bench marking.

Results: Our model correctly predicted whether EM images contained deposits with validation accuracy approaching 80% (graph and figure). Also it demonstrated validation accuracy close to 70% (graph) using only a small sample of our data limited to less than 100 of 512x512 pixel patches.

Figure 1 - 1606

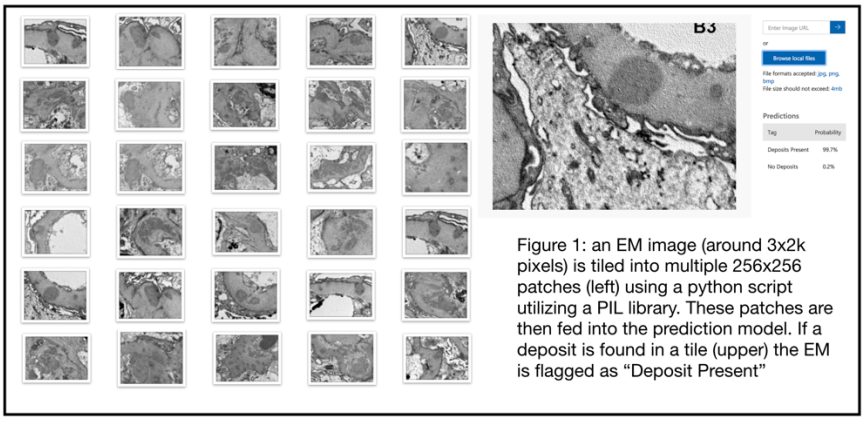

Figure 1: an EM image (around 3x2k pixels) is tiled into multiple 256x256 patches (left) using a python script utilizing a PIL library. These patches are then fed into the prediction model. If a deposit is found in a tile (upper) the EM is flagged as "Deposit Present"

Figure 2 - 1606

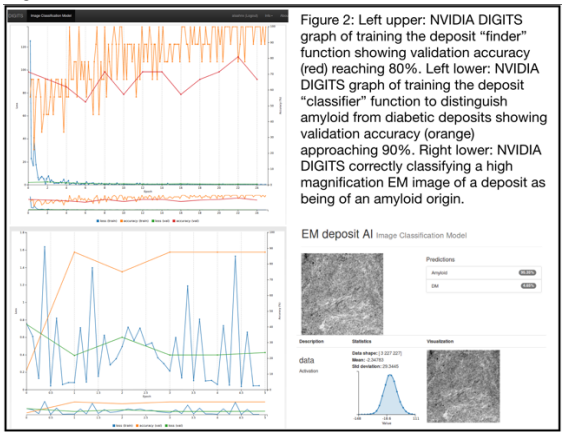

Figure 2: Left upper: NVIDIA DIGITS graph of training the deposit "finder" function showing validation accuracy (red) reaching 80%. Left lower: NVIDIA DIGITS graph of training the deposit "classifier" function to distinguish amyloid from diabetic deposits showing validation accuracy (orange) approaching 90%. Right lower: NVIDIA DIGITS correctly classifying a high magnification EM image of a deposit as being of an amyloid origin.

Conclusions: These results provide support for further studies addressing the potential use of deep learning approach as a tool identify and subclassify deposits in medical kidney disease. None the less, compared to published metrics, acceptable performance could be achieved leveraging publically available, easily accessibly deep learning platforms from major technology companies such as Google, Microsoft, and NVIDIA.

1607 Exostosin-1 and Exostosin-2 associated Membranous Lupus Nephritis

Aishwarya Ravindran[1], Benjamin Madden[1], Cristine Charlesworth[1], Fernando Fervenza[1], Sanjeev Sethi[1]
[1]Mayo Clinic, Rochester, MN

Disclosures: Aishwarya Ravindran: None; Benjamin Madden: None; Cristine Charlesworth: None; Fernando Fervenza: None; Sanjeev Sethi: None

Background: Membranous nephropathy (MN) is classified as primary and secondary. In primary MN, M-type phospholipase A2 receptor 1 (PLA2R) and Thrombospondin Type-1 Domain-Containing 7A were recently identified as target antigens. Secondary MN is usually associated with autoimmune diseases such as lupus. The target antigen in secondary MN is not known. The aim of this study was to determine the target antigen in membranous (class V) lupus nephritis (LMN).

Design: Utilizing our institutional database, we identified patients with diagnosis of LMN from January 2012 to April 2018. We identified 23 cases of LMN. We also identified 49 cases of proliferative lupus nephritis (LN) (class I-1 case, class II-7 cases, class III-6 cases, class IV-24 cases, and mixed III/IV with V- 11 cases). We used 23 PLA2R-positive MN as controls. We used laser microdissection and mass spectrometry (MS) to identify the target antigen and confirm the findings by immunohistochemistry (IHC).

Results: MS studies done in 6 of 23 cases of LMN showed high spectral counts of Exostosin I (EXT1) and Exostosin 2 (EXT2). The average spectral counts of EXT1 and EXT2 were 67.7 (SD ± 35.9) and 88.8 (SD ±41.4) (Figure 1). This was comparable to average PLA2R spectral count of 86.1 (SD ± 27.5) of PLA2R-positive MN. No spectra for EXT1 and EXT2 were identified in any case of pure LN (class I-IV) or PLA2R-positive MN; and only baseline PLA2R spectral counts (average 6.3) were present in EXT1/EXT2-positive LMN. EXT 1 and 2 are glycosyltransferases that exist as heterodimers and are responsible for the synthesis of the heparin sulfate backbone of the glomerular basement membrane (GBM). We next performed IHC for EXT1 and EXT2 in all cases of LMN, LN, and PLA2R-positive MN. Eleven (47.8%) of the 23 LMN cases, including the 6 positive by MS, showed bright granular staining for EXT1 and EXT2 along the GBM in a distribution similar to IgG (Figure 2). Three (27.2%) of the 11 cases of mixed LN and LMN were also positive of EXT1/EXT2. All cases of pure LN and PLA2R-positive MN were negative for EXT1/EXT2 staining. Finally, autoantibodies to EXT1 and heterodimer EXT1/EXT2 were detected in an index case of LMN and were negative in an index case of PLA2R-positive MN.

Figure 1 - 1607

Probability Legend:
over 95%
80% to 94%
50% to 79%
20% to 49%
0% to 19%

Bio View:
2732 Proteins in 2459 Clusters
With 2730 Filtered Out

	Accession Number	Molecular Weight	Protein Grouping Ambiguity	Combined_controls	Case 1	Case 2	Case 3	Case 4	Case 5	Case 6
Exostosin-2 OS=Homo sapiens GN=EXT2 PE=1 SV=1	sp|Q93063|EXT2_HUMAN	82 kDa		0	110	102	19	74	86	142
Exostosin-1 OS=Homo sapiens GN=EXT1 PE=1 SV=2	sp|Q16394|EXT1_HUMAN	86 kDa	*	(0)	94	75	11	40	78	108
Ig gamma-1 chain C region OS=Homo sapiens GN=IGHG1 PE=1 SV=1	sp|P01857|IGHG1_HUMAN	36 kDa	*	62	129	135	71	106	129	119
Ig gamma-2 chain C region OS=Homo sapiens GN=IGHG2 PE=1 SV=2	sp|P01859|IGHG2_HUMAN	36 kDa	*	49	70	100	44	77	88	97
Ig gamma-3 chain C region OS=Homo sapiens GN=IGHG3 PE=1 SV=2	sp|P01860|IGHG3_HUMAN	41 kDa	*	50	72	111	46	66	96	85
Ig gamma-4 chain C region OS=Homo sapiens GN=IGHG4 PE=1 SV=1	sp|P01861|IGHG4_HUMAN	36 kDa	*	24	116	68	33	72	70	40
Secretory phospholipase A2 receptor OS=Homo sapiens GN=PLA2R1 PE=1 SV=2	sp|Q13018|PLA2R_HUMAN	169 kDa	*	6	10	8	10	2	8	(0)

Figure 2 - 1607

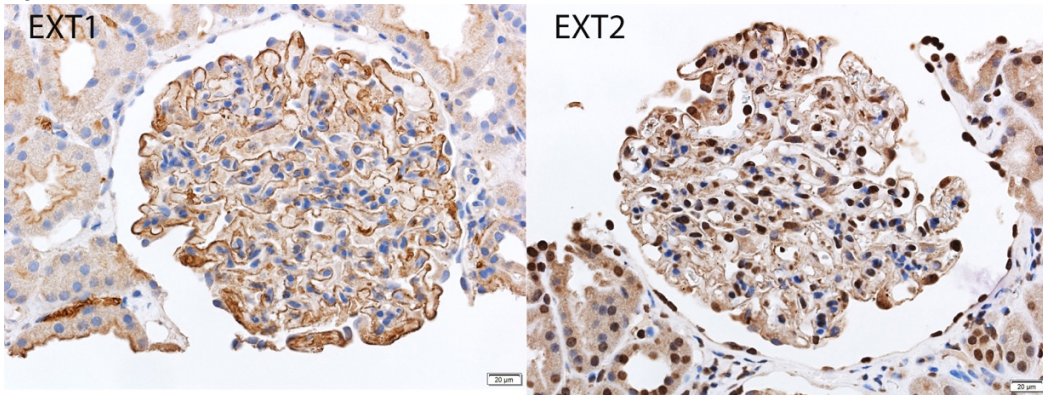

Conclusions: We show bright granular GBM staining for EXT1/EXT2 in 47.8% of LMN and negative staining in PLA2R-positive MN; EXT1/EXT2 are the likely target antigens in a significant number of LMN.

1608 Characterization of Membranous Nephropathy with Microspherular Deposits

Kevin Ren[1], Cynthia Nast[1], Jean Hou[2]
[1]Cedars-Sinai Medical Center, Los Angeles, CA, [2]Cedars Sinai Medical Center, Los Angeles, CA

Disclosures: Kevin Ren: None; Cynthia Nast: None; Jean Hou: None

Background: Membranous nephropathy (MN) is a common cause of adult nephrotic syndrome in the US. The typical ultrastructural finding is of subepithelial uniformly electron dense immune complex deposits along the glomerular basement membrane (GBM). There are few case reports and series of MN describing subepithelial deposits with a unique microspherular substructure that resembles, but does not contain proteins of, nuclear pores [Figure1]. Currently, the nature, composition, and clinical significance of these microspherular deposits (MSD) remain unknown. There have been no previous studies on the PLA2R and THSD7A status, or IgG subclass staining in MN with MSD, which may provide important etiologic and prognostic information on this rare but unique subset of MN.

Design: We retrospectively identified 16 MN biopsies with GBM deposits comprised either partially or wholly of aggregates of MSD by electron microscopy (EM). On EM examination, the location, distribution and size of the MSD were collected. 12 biopsies from 11 patients had global MSD accounting for >50% of all deposits. The 4 remaining biopsies had segmental MSD and were excluded from the study. Immunohistochemical staining for PLA2R and THSD7A, and immunofluorescence staining for IgG subclasses were performed to investigate the association of MSD with primary or secondary MN. Patient data were reviewed for potential causes of secondary MN.

Results: MSD were found in subepithelial (n=12), intramembranous (n=9), and less often mesangial (n=4) locations. Eleven biopsies (92%) showed Ehrenreich-Churg stage II or above. By EM, the microspherules had a mean diameter of 77.9 nm. All 12 biopsies were negative for PLA2R. Only 1 was positive for THSD7A, and no underlying malignancy was identified. IgG1 was the dominant subclass in 11 biopsies; and 1 biopsy had no tissue for subclass staining. One patient had 2 biopsies done four years apart, both of which had MSD and showed progression from Ehrenreich-Churg stage I to IV. Clinical and pathologic features are summarized in Table 1.

Table 1. Clinical and pathologic features of membranous nephropathy with microspherular deposits.

Patient No.	Age (y)/Gender	Clinical presentation	Concurrent medical conditions	Renal pathology diagnosis	Extent of MSD	Location of MSD	Stage	PLA2R	THSD7A	Capillary IgG	Dominant IgG subclass
1	45/M	Proteinuria	N/A	Membranous glomerulonephritis	>80 %	Subepithelial Intramembranous	3	N/A	N/A	N/A	N/A
2	75/F	Proteinuria, hematuria, elevated creatinine	+ANA	Membranous glomerulonephritis	>90 %	Subepithelial	2	Negative	Negative	2-3+ granular	IgG1, 2+
3	46/M	Nephrotic syndrome, hematuria	Hypertension	Membranous glomerulonephritis	100 %	Subepithelial Intramembranous	2	Negative	Negative	2-3+ granular	IgG1, 2+
4 (Biopsy1)	61/F	Nephrotic syndrome, hematuria	Hypertension	Membranous glomerulonephritis	100 %	Subepithelial	1	Negative	Negative	Trace-1+ granular	IgG1, trace-1+
4 (Biopsy2)	66/F	Recurrent proteinuria with known membranous nephropathy	Hypertension	Inactive membranous nephropathy	>80 %	Subepithelial Intramembranous	4	Negative	Negative	Trace granular	IgG1, trace
5 Allograft	58/M	Proteinuria, elevated creatinine	HCV infection	Membranous glomerulonephritis	>90 %	Subepithelial Intramembranous Mesangial (occasional)	4	Negative	Negative	Trace granular	IgG1, trace
6	43/F	Recurrent proteinuria with known membranous nephropathy	N/A	Advanced Membranous glomerulonephritis	100 %	Subepithelial Intramembranous Mesangial (frequent)	3	Negative	Negative	3+ granular	IgG1, 3+
7	57/F	Proteinuria	N/A	Membranous nephropathy	100 %	Subepithelial Intramembranous Mesangial (occasional)	3	Negative	Negative	2+ granular	IgG1, 1+
8	88/F	Nephrotic range proteinuria	Hypertension Hypothyroidism Negative GN serology	Membranous nephropathy	100 %	Subepithelial Intramembranous	3	Negative	Negative	3+ granular	IgG1, 3+
9	61/M	Progressive proteinuria	Hypertension Dyslipidemia	Membranous nephropathy	100 %	Subepithelial Intramembranous	3	Negative	Negative	3+ granular	IgG1, 2-3+
10	58/M	Proteinuria	Hypertension Diabetes Dyslipidemia Negative GN serology	Membranous nephropathy	100 %	Subepithelial Intramembranous Mesangial (occasional)	3	Negative	Positive	2-3+ granular	IgG1, 2-3+
11	41/F	Heavy proteinuria, hematuria	SLE	Membranous lupus nephritis, ISN/RPS Class V	50-60%	Subepithelial	3	Negative	Negative	1+ granular	IgG1, 2+

Abbreviation: MSD, microspherular deposits; N/A, not available; ANA, anti-nuclear antibody; HCV, hepatitis C virus; GN, glomerulonephritis; SLE, systemic lupus erythematosus; ISN/RPS, International Society of Nephrology/Renal Pathology Society.

Figure 1 - 1608

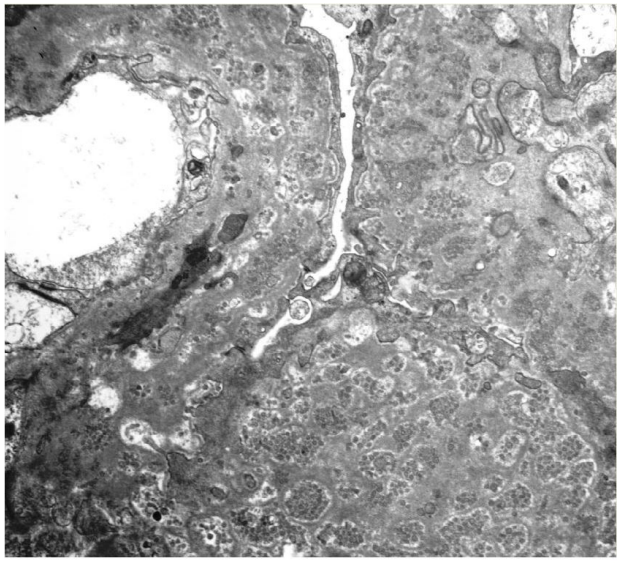

Figure 1. Subepithelial and intramembranous microspherular deposits. 14000x

Conclusions: MN with diffuse MSD represents a rare but distinct subset of MN, which most often is associated with IgG1 subclass dominance and negative PLA2R and THSD7A staining, suggesting association with secondary MN. It is possible MSD are associated with a specific MN antigen, requiring further investigation. MSD do not appear to be related to disease progression, as they were identified in a biopsy with early stage MN.

1609 A Comparison between the Percentage of Interstitial Fibrosis and Tubular Atrophy Foci (IFTA) and the Density of IFTA Foci on Kidney Wedge Sections

Luisa Ricaurte[1], Aleksandar Denic[1], R. Houston Thompson[1], Bradley Leibovich[1], Jonathan Munoz[1], Mariam Priya Alexander[1], Andrew Rule[1]
[1]Mayo Clinic, Rochester, MN

Disclosures: Luisa Ricaurte: None; Aleksandar Denic: None; R. Houston Thompson: None; Bradley Leibovich: None; Jonathan Munoz: None; Mariam Priya Alexander: None; Andrew Rule: None

Background: Interstitial fibrosis and tubular atrophy (IFTA) identifies the final histology of irreversibly damaged kidneys. The severity of IFTA is typically a semi-quantitative score by pathologists or quantitatively measured by morphometry as the percentage of the tissue that is IFTA (%IFTA). In our study, we developed a new approach in assessing fibrosis. The number of IFTA foci per cortex area (nIFTAf) was compared to %IFTA.

Design: We studied 842 patients with radical nephrectomy due to tumor from 2000 to 2012. Wedge sections were taken from the cortical kidney distal to the tumor, fixed in formalin, embedded in paraffin, cut into 3µm thick sections, stained with periodic acid-Schiff, and scanned into high resolution images. Based on visual inspection, a renal pathologist scored the percentage of cortex that was IFTA into 4 categories: <10%, 10-25%, 25-50% and >50%. Masked to this, the cortex was manual traced as well as all regions of IFTA to calculate %IFTA by morphometry. The nIFTAf was calculated as the number of traced IFTA foci normalized per 5mm^2 of cortex area (**Figure 1**). Clinical, biopsy, and contrast computerized tomography scan (CT scan) characteristics were correlated with the three IFTA measures (Spearman's correlation).

Results: The pathologist IFTA scoring correlated with %IFTA (r_s=0.47, p<0.0001). The nIFTAf showed stronger correlation with %IFTA (r_s=0.68, p<0.0001), though at high %IFTA, the nIFTAf decreased rather than increased as large IFTA foci became confluent (**Figure 2)**. After age adjustment, IFTA by all three methods associated with diabetes, proteinuria, lower estimated glomerular filtration rate (eGFR), and chronic changes on histology: %glomerulosclerosis, %ischemic glomeruli (among all non-sclerosed glomeruli) and %luminal stenosis from intimal thickening of the most orthogonal small-medium artery. These correlations were stronger by %IFTA, and only %IFTA associated with larger kidney volumes on CT scan (**Table 1)**. After %IFTA adjustment, more nIFTAf went from associating with lower eGFR to associating with higher eGFR and from associating with higher proteinuria to associating with lower proteinuria **(Table 2).**

Table 1. Age-adjusted correlation to clinical, biopsy and CT scan characteristics with three methods assessing IFTA

Characteristic	Pathology IFTA Score r_s (*p* value)	% IFTA r_s (*p* value)	nIFTAf r_s (*p* value)
BMI	0.07 (0.06)	0.11(0.003)	0.04 (0.22)
Diabetes	0.12 (0.008)	0.24 (<0.0001)	0.13 (0.0002)
Glucose	0.08 (0.07)	0.13 (0.003)	0.10 (0.03)
Hypertension	0.10 (0.001)	0.15 (<0.0001)	0.12 (0.0005)
Estimated GFR	-0.33(<0.0001)	-0.35 (<0.0001)	-0.16 (<0.0001)
24hr urine protein	0.25 (<0.0001)	0.32 (<0.0001)	0.12 (0.003)
% Glomerulosclerosis	0.29 (<0.0001)	0.52 (<0.0001)	0.41 (<0.0001)
% Ischemic glomeruli	0.32 (<0.0001)	0.46 (<0.0001)	0.30 (<0.0001)
% Luminal Stenosis	0.23 (<0.0001)	0.27 (<0.0001)	0.12 (0.0003)
Kidney volume*	0.04 (0.41)	0.14 (0.0004)	0.03 (0.43)
Cortex volume*	0.04 (0.37)	0.13 (0.001)	0.03 (0.40)
Medulla volume*	0.02 (0.66)	0.15 (<0.0001)	0.03 (0.44)

*Obtained from CT scan evaluation

Table 2. Comparison of two morphometric methods in assessing IFTA, after adjusting for age and each method

Characteristic	% Fibrosis Area r_s (*p* value)	# of Foci per 5 mm^2 r_s (*p* value)
BMI	0.10 (0.004)	-0.03(0.41)
Diabetes	0.21 (<0.0001)	-0.03 (0.44)
Glucose	0.09 (0.06)	0.02 (0.65)
Hypertension	0.09 (0.006)	0.04 (0.28)
Estimated GFR	-0.33 (<0.0001)	0.09 (0.01)
24hr urine protein	0.31 (<0.0001)	-0.09 (0.02)
Glomerular volume	0.11 (0.004)	-0.05 (0.23)
Tubular area (cortex)	0.15 (<0.0001)	-0.07 (0.07)
Tubular area (medulla)	0.22 (<0.0001)	-0.08 (0.03)
% Glomerulosclerosis	0.37 (<0.0001)	0.13 (0.0009)
% Ischemic glomeruli	0.37 (<0.0001)	0.02 (0.68)
% Luminal Stenosis	0.25 (<0.0001)	-0.06 (0.09)
Kidney volume*	0.15 (0.0003)	-0.07 (0.13)
Cortex volume*	0.13 (0.001)	-0.05 (0.21)
Medulla volume*	0.17 (<0.0001)	-0.08 (0.08)

*Obtained from CT scan evaluation

Figure 1 - 1609

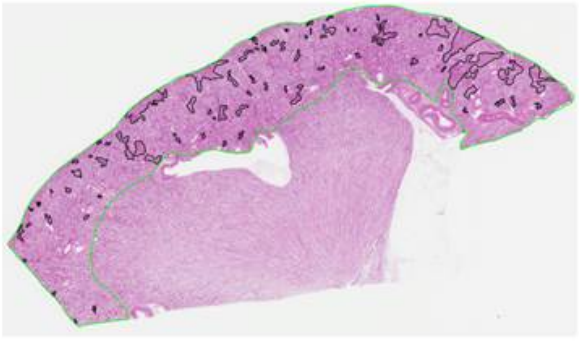

Figure 1. Renal wedge section with IFTA foci tracings in black, and cortex tracing in green.

Figure 2 - 1609

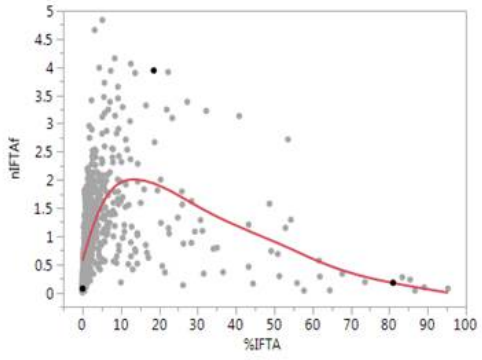

Figure 2. Correlation between nIFTAf and %IFTA. %IFTA is positively correlated to nIFTAf though at very high %IFTA, nIFTAf decreased as large IFTA foci became confluent.

Conclusions: Of the three methods for assessing IFTA, morphometric %IFTA has the strongest associations with pathology detected by clinical, biopsy, or CT scan evaluation. More IFTA foci at the same amount of %IFTA suggests a somewhat more benign chronic pathology with better kidney function.

1610 Hydrophilic Polymer Nephropathy Following Endovascular Procedures

Preethi Sekar[1], Alexander Gallan[2], Bradford West[3], Anthony Chang[4], Kammi Henriksen[4]
[1]University of Chicago Medicine, Chicago, IL, [2]Brookfield, IL, [3]Memorial Medical Center, Springfield, IL, [4]University of Chicago, Chicago, IL

Disclosures: Preethi Sekar: None; Alexander Gallan: None; Bradford West: None; Anthony Chang: None; Kammi Henriksen: None

Background: Hydrophilic polymer-coated devices including guidewires, stents, and catheters are widely used for intravascular procedures in order to improve maneuverability and prevent arterial spasm. However, there have been reports of hydrophilic polymer emboli (HPE) causing microvascular obstruction in various organs after endovascular procedures, most frequently the lung and brain. Such iatrogenic embolization can result in complications including ischemia, infarct, and death. The literature on renal HPE is sparse, with only 2 reported cases. We report a series of 4 cases of hydrophilic polymer nephropathy in order to better characterize the pathologic spectrum of kidney injury.

Design: We conducted a search of the pathology archives from January 2000 to August 2018 using the terms aortic stent, aortic aneurysm repair, and renal artery stent. After excluding infrarenal aortic aneurysms, we identified 22 patients (20 autopsies and 2 kidney biopsies) who had undergone endovascular interventions. Clinicopathologic features were reviewed.

Results: HPE were present in 4 cases (18%), including 3 autopsies and 1 allograft kidney biopsy, summarized in the table. HPE were identified in glomerular capillaries and hilar vessels, arterioles, interlobular arteries, and peritubular capillaries. The HPE were pale basophilic with an amorphous to granular texture (non-refractile, non-polarizable). Focally they had a serpiginous structure. There was no associated inflammation or giant cell reaction. In cases 1 and 2, the HPE were associated with fibrin-platelet thrombi. In cases 1, 2, and 4 there were features of acute tubular injury. All cases showed moderate to severe arteriosclerosis and varying degrees of tubulointerstitial scarring. None of the cases contained atheroemboli.

Case	Age/sex	Comorbid conditions	Intravascular procedures (and time prior to biopsy/death)	Lab values at time of biopsy/death	Specimen
1	68/F	CAD, CKD, DM, HTN, COPD, TAAA	AAA repair with celiac, SMA, and bilateral renal artery stents (8 days) Coronary artery stents (~3 years)	SCr - 2.5 mg/dL	Autopsy
2	65/M	HTN, CAD, CKD, CVA, Type 2 TAAA	AAA repair with thoracic aortic and aortoiliac stents (2 days)	SCr- 3.0 mg/dL	Autopsy
3	65/M	RCC, HTN, DM, Type IV TAAA	AAA repair with celiac, SMA, and renal artery stents (1.9 years)	SCr - 4.3 mg/dL	Autopsy
4	50/M	Type 1 DM, ESRD s/p kidney transplant	Iliofemoral endarterectomy with angioplasty and lower extremity thromboembolectomy (1.5 months)	SCr - 2.1 mg/dL	Kidney allograft biopsy

Figure 1 - 1610

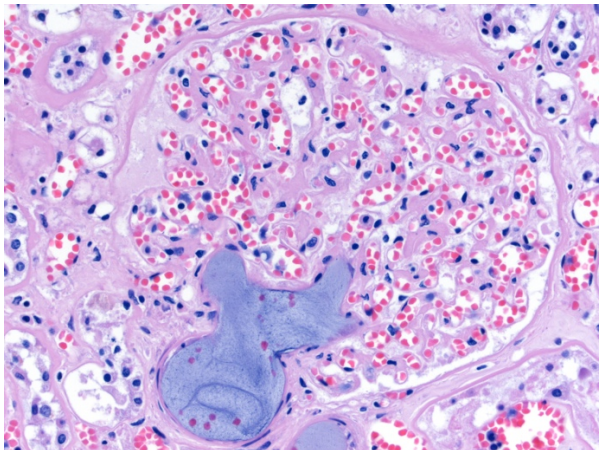

Figure 2 - 1610

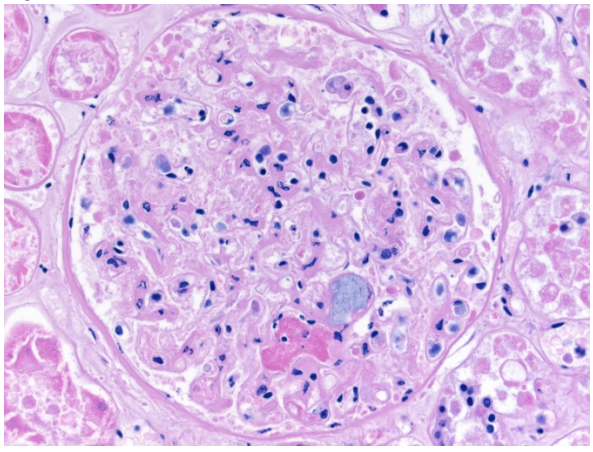

Conclusions: HPE is an under-recognized phenomenon despite widespread use of polymer coated devices. We report the first case series of hydrophilic polymer nephropathy following endovascular procedures. HPE demonstrate a characteristic basophilic amorphous appearance and can be identified in different caliber vessels in the renal cortex including glomerular and peritubular capillaries, arterioles, and arteries. The spectrum of changes in hydrophilic polymer nephropathy also includes acute thrombotic microangiopathy and acute tubular injury, which may result in permanent sequelae. In addition to atheroemboli, iatrogenic polymer embolization should be considered as a potential complication following vascular intervention.

1611 Podocyte protrusions into glomerular basement membrane (GBM) and GBM defects are common in glomeruli from proteinuric diabetic nephropathy (DN) patients and are strong predictors of albuminuria

Xiao Xia Tiffany Shao[1], Behzad Najafian[1], Jonathan Jefferson[1], Abbal Koirara[2], Michael Mauer[3], Robert Nelson[4]
[1]University of Washington, Seattle, WA, [2]UW Medical Center, Seattle, WA, [3]University of Minnesota, Minneapolis, MN, [4]National Institute of Health, Phoenix, AZ

Disclosures: Xiao Xia Tiffany Shao: None; Michael Mauer: None; Robert Nelson: None

Background: GBM thickening is a defining feature of DN. Other forms of GBM abnormalities, such as podocyte protrusions into GBM (PPIG) are occasionally seen in DN biopsies. We studied biopsies from DN patients and correlated these additional GBM lesions with other DN structural parameters and albumin/creatinine ratio (ACR).

Design: Electron microscopy (EM) images from 25 clinical kidney biopsies with DN primary diagnosis were studied. In order to better understand relationships between GBM abnormalities and DN severity, research biopsies from 5 normoalbuminuric (NA), 5 microalbuminuric (MA) and 5 proteinuric (P) type 2 diabetic patients were studied by EM. GBM abnormalities were classified as PPIG, GBM defects (GBMD) with or without capillary loops with thin basement membranes (CLTBM), intra-GBM cytoplasmic elements (ICE), focal GBM lucencies (FGL), and GBM lamellation (**Figure 1**), and quantified per capillary loop (/CL). GBM width, fractional volume of mesangium per glomerulus [Vv(Mes/glom)], foot process width (FPW), and fractional volume of interstitium per cortex [Vv(Int/cortex)] were quantified by morphometry.

Results: 87±44 and 196±105 CL per biopsy were examined in clinical and research biopsies, respectively. The majority of clinical biopsies showed severe DN. All clinical and research biopsies showed PPIG and ICE. Some PPIGs had FGL at the base of the protruding podocyte. GBMD was present in 56% of clinical (~3/100 CL) and 33% of research biopsies (all P and 1/5 MA cases). All GBMDs were covered by CLTBM, irregular matrix, or podocytes making direct contact with endothelial or mesangial cells. FGL and segmental lamellation were common. In clinical biopsies, % segmental sclerosis correlated with ICE/CL (R=0.54, p=0.02), GBM lamellation (R=0.71, p=0.001), and GBM abnormalities combined (R=0.53, p=0.02). GBM abnormalities combined were >5 fold more common in P *vs.* MA and NA patients (**Figure 2**). Correlations between GBM abnormalities and other variables are shown in the **Table**. By multiple regression analysis, GBM abnormalities alone explained 85% of ACR variability, while classical DN lesions including GBM width and Vv(Mes/glom) explained 48% of ACR variability.

	GBM width	Vv(Mes/glom)	FPW	Vv(Int/cortex)	ACR
PPIG/CL	0.62, 0.01	0.55, 0.04	NS	NS	0.64,0.01
(PPIG >1/2) /CL	NS	NS	0.57, 0.03	NS	NS
GBMD/CL	0.58, 0.02	NS	NS	0.59, 0.02	0.81, 0.0001
FGL/CL	NS	NS	NS	NS	0.71, 0.003
ICE/CL	0.65,0.008	0.53, 0.04	NS	NS	0.71, 0.003
FGL at base of PPIG	0.67, 0.007	0.62, 0.01	NS	NS	0.88,0.0001
GBM lamellation/CL	NS	NS	NS	NS	0.60,0.02
Any GBM abnormalities	0.64,0.01	0.53,0.04	NS	0.51, 0.05	0.74,0.002

Table. Correlations between GBM abnormalities and structural parameters reflecting diabetic nephropathy, podocyte injury and interstitial fibrosis, and albuminuria. All values are presented as correlation "R, p-value". NS = statistically not significant.

Figure 1 - 1611

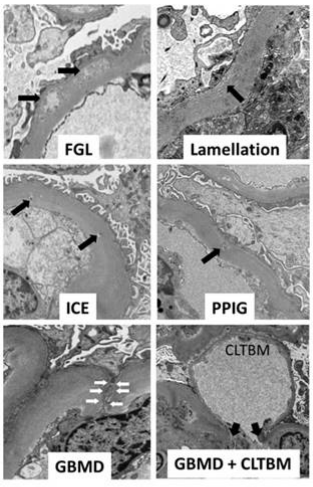

Figure 1. GBM structural abnormalities (marked by arrows)

Figure 2 - 1611

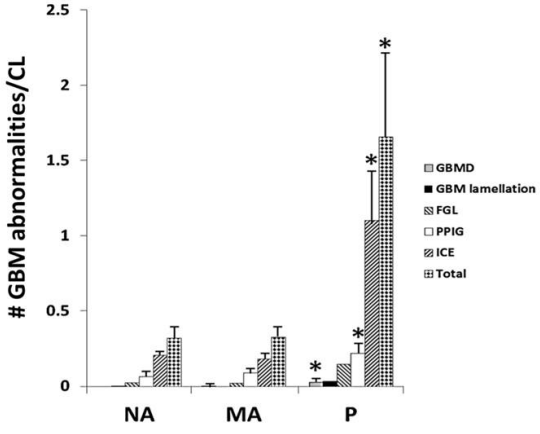

Figure 2. Prevalence of GBM abnormalities in normoalbuminuric (NA), microalbuminuric (MA) and proteinuric (P) type 2 diabetic patients. *p<0.05

Conclusions: DN is associated with GBM structural abnormalities that are more prevalent in proteinuric patients and are likely to play significant roles in the progression of DN as evidenced by their strong association with ACR, and correlations with GBM width, mesangial expansion, segmental sclerosis, and interstitial fibrosis.

1612 Glomerular Basement Membrane (GBM) Thickness Variability in Biopsies with Thin Basement Membrane Disease (TBMD)

Xiao Xia Tiffany Shao[1], Gianni Niolu[1], Charles Alpers[2], Kelly Smith[1], Shreeram Akilesh[1], Roberto Nicosia[3]
[1]University of Washington, Seattle, WA, [2]University of Washington School of Medicine, Seattle, WA, [3]VA Puget Sound Health Care System, Seattle, WA

Disclosures: Xiao Xia Tiffany Shao: None; Gianni Niolu: None; Charles Alpers: None; Kelly Smith: None; Shreeram Akilesh: None

Background: TBMD although associated with a benign course in majority of patients can progress in some leading to chronic kidney disease. While TBMD diagnosis relies on GBM thickness measured by electron microscopy (EM), there is no general consensus for how to measure average GBM thickness and thresholds obtained by various methods. In order to determine the proper sampling strategy for obtaining average GBM thickness, we studied the variability within and among capillary loops and glomeruli in biopsies with TBMD.

Design: Ten kidney biopsies diagnosed as TBMD were studied. All available glomeruli in the thin sections and all available capillary loops were studied by EM (~20,000 x). The protocol proposed by Haas (Arch Pathol Lab Med. 2009;133:224–232) was used and 3 measurements were made per capillary loop. The plots of individual vs. average measurements per capillary loop and per glomerulus were prepared and variance component analysis was performed. Using the threshold for diagnosing TBMD (215-235 nm) in adults proposed by the Haas study, the number of measurements needed to reach <5% error (difference from biopsy mean obtained from all measurements) corresponding to ~10 nm was determined.

Results: 210 [96-324], median [range], measurements were performed in 70 [32-108] capillary loops from 4[2-6] glomeruli per biopsy. The median GBM thickness among the biopsies was 186 [163-224] nm. There was significant variability in GBM thickness between individual capillary loops. In order to obtain <5% error, the median number of GBM measurements needed was 38 [4-71] and the median number of capillary loops needed was 15 [2-27] (**Figure 1**). Variance component analysis showed that except in one outlier, the major portion of GBM thickness variability resided in differences between measurements within a given capillary loop (56±9%) and between different capillary loops within the same glomerulus (37±10%), rather than between different glomeruli within a biopsy (7±6%). The outlier had 2 glomeruli with average GBM thicknesses of 254 and 181 nm and greater variance between the glomeruli than between capillary loops or within a capillary loop.

Figure 1 - 1612

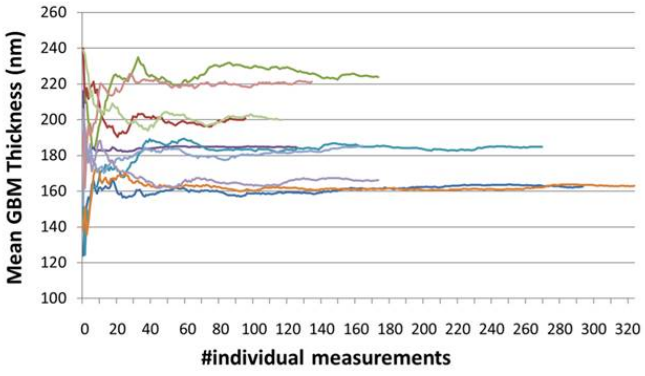

Figure 1. Mean GBM thickness vs. number of individual thickness measurements in 10 biopsies with TBMD.

Figure 2 - 1612

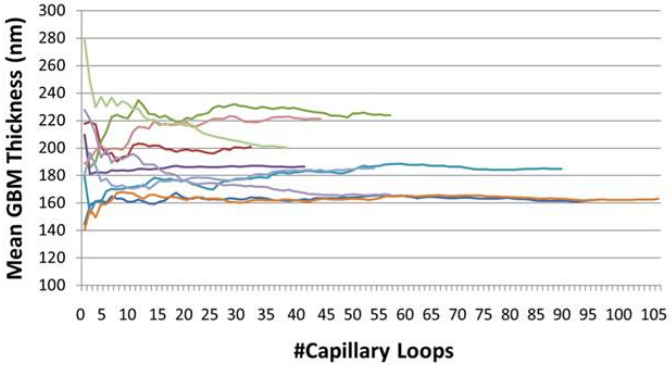

Figure 2. Mean GBM thickness vs. number of capillary loops measured in 10 biopsies with TBMD.

Conclusions: We propose that 40 measurements distributed among 15 capillary loops should provide a robust average GBM thickness measurement in a biopsy. However, substantial differences in GBM thickness variability exists between and within capillary loops. Significance of this variability is currently not known.

1613 Plasma Endothelial Microvesicles (EMV) with IgG Binding Increase in Antibody Mediated Rejection (AMR): A Potential Explanation for Negative IgG staining in Peritubular Capillaries (PTC)

Xiao Xia Tiffany Shao[1], Behzad Najafian[1], Christopher Blosser[1], Nicolae Leca[2], Indhira De la cruz Alcantara[2]
[1]University of Washington, Seattle, WA, [2]UW Medical Center, Seattle, WA

Disclosures: Xiao Xia Tiffany Shao: None; Indhira De la cruz Alcantara: None

Background: AMR is caused by donor specific antibodies (DSA) of mainly IgG type; however, PTC typically do not show IgG staining in AMR. Here, we report a case of C4d+ AMR with transient IgG staining in PTC. We hypothesized that allograft endothelial cells release their bound IgG to blood through EMVs. To test this, we studied plasma EMV in kidney transplant patients with or without AMR.

Design: A 61-year-old woman with a history of prior kidney transplant and 100% PRA+ received a second transplant. A surge in DSA led to a biopsy on day 9 post-transplant. Platelet poor plasma (PPP) from this patient and 8 other AMR cases, 9 kidney transplants with no AMR (NAMR) and 9 healthy controls (HC) were compared for (C4d+)EMV, (C4d+) annexin-V binding microvesicles [(C4d+)ABVMV] by flow cytometry.

Results: The day-9 biopsy was unremarkable by light microscopy, with no significant microvascular inflammation and no T-cell mediated rejection. However, there was diffuse staining for C4d, IgG, C3 and C1q in PTC by immunofluorescence suggestive of AMR (**Figure**

1). The patient was treated for AMR, which resulted in improved renal function. A follow up biopsy on day-45 showed mild acute T-cell mediated rejection, prominent glomerulitis and peritubular capillaritis and diffuse weak C4d and very modest C1q, but no IgG or C3 staining in peritubular capillaries. Imaging flow cytometry showed co-localization of IgG on about ~11% of EMV in AMR subjects vs. only ~1% of EMV in NAMR (p=0.01) and ~0.5% of EMV in HC (p=0.009). (IgG+)EMV concentration was greater in AMR vs. NAMR (16 fold, p=0.08) and HC (27 fold, p=0.002). %IgG(+)EMV correlated with (C4d+)ABVMV (r=0.53, p=0.0001) and sum DSA class II (r=0.45, p=0.016), but not DSA class I. In addition, (C4d+)EMV concentration was greater in AMR vs. NAMR (16 fold, $p=10^{-6}$) and HC (44 fold, $p=10^{-6}$). (C4d+)ABVMV was also greater in AMR vs. NAMR (4 fold, p=0.056) and HC (10 fold, p=0.005). (C4d+)EMV concentration in the present case was 6168/µl, which was reduced to 748/µL following treatment.

Figure 1 - 1613

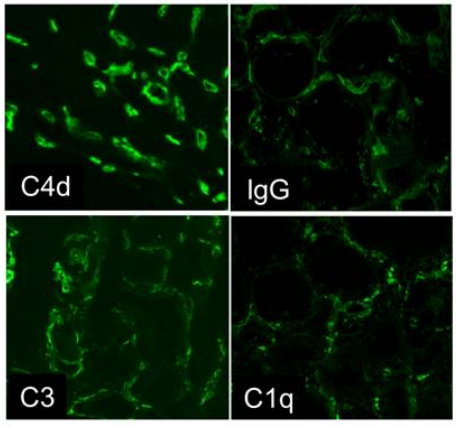

Figure 1. Day-9 biopsy with PTC staining for C4d, IgG, C3 and C1q.

Figure 2 - 1613

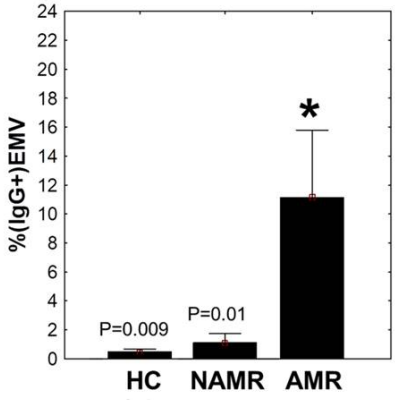

Figure 2. %(IgG+)EMV was significantly greater in AMR compared to NAMR or HC subjects.

Conclusions: To our knowledge this is the first reported case of AMR with IgG staining in PTC (in addition to C4d), but IgG staining was transient. Prominent increase in plasma (IgG+)EMV and (C4d+)EMV in AMR cases and correlations between (IgG+)EMV and (C4d+) are supportive of the hypothesis that allograft endothelial cells release bound IgG to the blood through EMV, perhaps as a protective mechanism.

1614 Post-Transplant Lymphoproliferative Disorder and Graft Versus Host Disease in Adult and Pediatric Patients with Liver, Kidney, and Intestinal Transplants: a 17-Year Single Institution Experience

Amy Starr[1], Alicia Henao Velasquez[2], Kyungmin Ko[2], Bhaskar Kallakury[3]
[1]Alexandria, VA, [2]MedStar Georgetown University Hospital, Washington, DC, [3]Georgetown University Hospital, Washington, DC

Disclosures: Amy Starr: None; Alicia Henao Velasquez: None; Kyungmin Ko: None; Bhaskar Kallakury: None

Background: Post-transplant lymphoproliferative disorder (PTLD) and graft versus host disease (GvHD) are infrequent complications in transplant patients, especially in solid organ and bowel transplant. Knowledge of these two diseases has come from smaller retrospective studies. Our hospital is one of the largest transplant centers in the U.S. performing approximately 5,100 kidney, liver, and intestinal transplants in pediatric and adult populations over 17 years.

Design: Patients diagnosed with PTLD and GvHD from 2001-2018 were identified using the search functions in Cerner and Powerpath. Electronic chart review was performed on each patient. The clinical and pathological aspects of these two disorders were analyzed.

Results: PTLD was identified in 49 patients, with an estimated overall incidence of 1% and median follow up of 6.3 years. PTLD was most common in intestinal/multivisceral transplant (47%) followed by liver (37%) and kidney (14%). The most common PTLD type was monomorphic (54%), followed by early lesion (24%) and polymorphic (22%). Half of these patients developed PTLD within one year. Adults were more commonly affected than pediatric patients (61% versus 39%). There was no difference in survival between polymorphic and monomorphic PTLD (p=0.68).

GvHD was identified in 27 patients, with an estimated overall incidence of 0.5% and median follow up of 15 months. The most common transplant type associated with GvHD was multivisceral/intestinal transplant (78%) compared to liver and kidney transplants (22%,

p=0.003). Although there was no difference in age of onset, incidence was higher in males (67% vs 33%). Gastrointestinal tract and skin were most frequently involved (81%). Majority of these patients were alive (56%) compared to those who died of GVHD (19%) at last follow-up (table 1).

Six patients (8.6%) were diagnosed with both PTLD and GvHD. Four patients developed GVHD after diagnosis of PTLD, and two of these patients died of progressive GvHD. Two patients were diagnosed with GvHD before developing PTLD, and one of these patients died of progressive GVHD. Patients with PTLD were 24 times more likely to have GvHD than patients without PTLD (p<0.0001).

PTLD		GvHD	
49 total cases		27 total cases	
Transplant type	***n*/percentage**	**Transplant type**	***n*/percentage**
Intestinal/multivisceral	23/47	Intestinal/Multivisceral	21/77
Liver	18/37	Liver	4/15
Kidney	7/14	Kidney	1/4
Liver and kidney	1/2	Liver and Kidney	1/4
PTLD Type		**Age group**	
Monomorphic	13/27	Adult	13/48
Polymorphic	11/22	Pediatric	14/52
Non-destructive	12/24	**Gender**	
Age group		Male	18/67
Adult (>20yrs)	30/61	Female	9/33
Pediatric	19/39	**Grade**	
Gender		1	13/48
Male	27/55	2	8/30
Female	22/45	3	4/15
CD20 status		4	2/7
Positive	43/88	**Type**	
Negative	6/12	Acute	16/59
EBER		Chronic	11/41
Positive	44/90	**Organs involved**	
Negative	3 (2 insufficient)/6	Skin	20
Prior acute rejection		GI	17
Yes	17/35	Bone marrow	2
No	32/65	Lung	1
Outcome of graft		Liver	1
Lost due to PTLD	3/6	Pancreas	1
Lost due to rejection	8/16	**Patient outcome**	
Retained	19/39	Alive	14/52
Patient outcome		Died due to GvHD	5/18
Alive	28/58	Other cause of death	4/15
Died due to PTLD	7/14	Lost to follow up	4/15
Other cause of death	7/14		
Lost to follow up	7/14		

Conclusions: Graft/patient survival in PTLD remains high and not affected by histologic subtype, likely a result of advanced therapeutic strategies. Survival from GvHD is similarly relatively high, except in those who have both diseases. Our data confirms the strong association between PTLD and GvHD, but shows an overall low incidence.

1615 Vancomycin-related nephropathy: Comprehensive evaluation of 36 biopsies

Ngoentra Tantranont[1], Yosu Luque[2], Roberto Barrios[3], Lillian Gaber[3], Luan Truong[4]
[1]The Houston Methodist Hospital, Houston, TX, [2]Sorbonne University, Assistance Publique Hôpitaux de Paris, Paris, France, [3]The Methodist Hospital, Houston, TX, [4]Houston Methodist Hospital, Houston, TX

Disclosures: Ngoentra Tantranont: None; Yosu Luque: None; Roberto Barrios: None; Luan Truong: None

Background: Vancomycin (V) is the choice for treating bacterial infection resistant to traditional antibiotics. V-associated nephrotoxicity (VaN) is well documented. However, the renal changes in VaN are poorly understood, reflecting a body of literature of only about 19 previous renal biopsy case reports. Vancomycin (V) is the choice for treating bacterial infection resistant to traditional antibiotics. V-associated nephrotoxicity (VaN) is well documented. However, the renal changes in VaN are poorly understood, reflecting a body of literature of only about 19 previous renal biopsy case reports.

Design: Data of kidney biopsies who had V administration since 2010 were collected.

Results: Thirty-six renal biopsies with VaN were identified from 1,828 native kidney biopsies from the Renal Pathology Laboratory, The Houston Methodist Hospital/ Baylor College of Medicine. The clinical profiles included age 23-84 years (mean 54), F/M ratio 15/11, diabetes 16, hypertension 12, marked obesity 2, and HIV infection 2. The patients had history of infection, particularly at skin and subcutis. Acute kidney injury was noted in all, nephrotic-range proteinuria in 2, skin rash in 1, and nephrotoxic agents in 7. Other diseases were also noted, including diabetic nephropathy (16), arterial nephrosclerosis 18, FSGS 1, IgA nephropathy 1, myoglobin casts 3, post-infectious GN 1, cholesterol embolism 1. The V-related renal changes included acute tubular necrosis (ATN) in 9 (25%), acute tubulointerstitial nephritis (ATIN) in 6 (17%), and ATIN with prominent acute tubular cell injury in 20 (56%). Fourteen biopsies (39%) showed tubular casts with distinctive morphologic features and tubular casts with some of these features in another 13 biopsies (36%). One (3%) showed neither ATN nor ATIN but chronic tubulointerstitial injury associated with arterial nephrosclerosis. Immunostain for V and uromodulin showed uniform V deposition in both typical and atypical casts. Coprecipitation of V and uromodulin was also noted. EM showed in 12 biopsies characteristic features of V casts: laminated appearance or spherules with denser outer rim, often present in the fibrillary background of uromodulin.

Conclusions: VaN is increasingly identified in renal biopsies. Diabetes seems to a major risk factor. VaN is manifested by either ATN or ATIN or both in a single biopsy. Tubular casts composed of co-precipitated V and uromodulin with a distinctive LM and EM features are frequent, with a significant diagnostic and pathogenetic implication.

1616 Renal Biopsy Specimen Adequacy and Non-Diagnostic Frequency

Andrew Tharp[1], Kimberly Collins[2], Carrie Phillips[2], Michael Eadon[2]
[1]Indiana University School of Medicine, Evansville, IN, [2]Indiana University School of Medicine, Indianapolis, IN

Disclosures: Andrew Tharp: None; Kimberly Collins: None; Carrie Phillips: None; Michael Eadon: None

Background: A kidney biopsy specimen plays an integral role in diagnosis and management of renal disease, but is costly and labor-intensive, exposing a patient to possible morbidity and mortality. Specimens may be of limited diagnostic potential due to insufficient glomeruli. To avoid risks of a repeat biopsy procedure, pathologists must decide how to best utilize resources for additional section preparation to improve diagnostic yield in samples with limited tissue. These extra efforts are usually unreimbursed. We sought to determine the impact of specimen adequacy on diagnostic frequency, as well as whether mapping of multiple sequential paraffin tissue sections improves glomerular yield or alters the proportion of obsolescent glomeruli identified.

Design: We retrospectively interrogated an electronic database of all renal biopsy specimens examined in an academic health system between 2002 and 2017. In 6943 specimens, we compared the ability to render a diagnosis based on glomerular counts reported for light microscopy. In a subgroup of 207 randomly selected cases that underwent more extensive mapping of eight tandem histological slides, we assessed paraffin sections for additional glomerular yield, diagnostic frequency, and change in glomerular obsolescence. Chi-square and t-tests were computed.

Results: Of the 6943 cases, paraffin sections in 2554 cases contained 13 or fewer glomeruli, 942 contained 7 or fewer glomeruli, 6776 were diagnostic and 167 were non-diagnostic. In specimens with ≥ 14 glomeruli, 1.3% were non-diagnostic compared to 4.2% of specimens with ≤ 13 ($p \leq 0.001$) and 9.3% with ≤ 7 glomeruli ($p \leq 0.001$). Mapping of multiple sequential paraffin sections in 207 specimens improved glomerular yield by 6.7 ± 0.5 glomeruli as compared to a single Periodic Acid Schiff-stained section, but only 3.5 ± 0.5 in specimens with ≤7 glomeruli (N=48). No significant change in diagnostic frequency or degree of glomerular obsolescence was appreciated among all 207 specimens with additional sequential mapping ($p = 0.13$) or the 48 specimens with ≤7 glomeruli ($p = 0.16$).

Conclusions: Number of glomeruli in a renal biopsy specimen predicts the specimen's diagnostic potential. Mapping of additional sequential sections modestly improves glomerular yield, but burdens the pathologist with unreimbursed time and effort, and does not significantly improve diagnostic frequency or change glomerular obsolescence.

1617 Pregnancy-Related Renal Disease: A 10-Year Perspective

Karen Trevino[1], Carrie Phillips[1]
[1]Indiana University School of Medicine, Indianapolis, IN

Disclosures: Karen Trevino: None; Carrie Phillips: None

Background: Kidney injury is serious complication in pregnancy resulting in significant morbidity and mortality, including fetal loss. Underlying etiologies during pregnancy may be shifting over the last several decades due to improved prenatal care, decrease in septic abortions, and increase in average maternal age.

Design: We retrospectively searched an electronic database of surgical pathology specimens for the past ten years to identify kidney biopsy specimens obtained during pregnancy or in the postpartum period. Pathology reports, slides and medical records were reviewed. We recorded age, race, primary glomerular diagnosis, degree of interstitial fibrosis and tubular atrophy, blood pressure, and available

laboratory data (such as urinalysis, serology, and creatinine) to help support the histologic diagnosis. Most recent available creatinine and need for renal replacement therapy were recorded as endpoints.

Results: We identified 36 cases of which 11 were diagnosed as IgA nephropathy (31%), 7 focal segmental glomerulosclerosis (19%), 5 nodular diabetic glomerulosclerosis (14%), 3 lupus nephritis (8%), 3 minimal change disease (8%), 2 acute tubular necrosis (6%), 2 interstitial nephritis (6%, one granulomatous), and one case each (3%) of glomerular capillary endotheliosis, diffuse crescentic glomerulonephritis, and anti-glomerular basement membrane disease. Adequate follow-up data was available in 24 cases. Eight patients required long term renal replacement therapy (n = 4 dialysis, n = 4 transplant) and one required short term therapy. Of those requiring long term therapy, 4 had nodular glomerulosclerosis, 2 focal segmental glomerulosclerosis, 1 acute tubular necrosis, and 1 IgA nephropathy. Thus, 4 of the 5 patients (80%) with nodular glomerulosclerosis required long term renal replacement therapy.

Conclusions: In our cohort of patients, nearly one-third had IgA nephropathy. This may be due to the likelihood that young, asymptomatic patients may first receive access to healthcare with laboratory screening during pregnancy. Nearly a quarter of patients demonstrated renal involvement from systemic diseases, such as lupus or diabetes mellitus. Lastly, diabetics with glomerulosclerosis demonstrated a high likelihood to progress to end stage renal disease requiring renal replacement therapy and represented half of our patients that progressed to this degree. Given the diversity of diagnoses in this population, renal biopsy may be justified to guide treatment decisions.

1618 Repeat Kidney Biopsy in Patients with Lupus Nephritis: Class-Switching and Progression of Chronicity

Vighnesh Walavalkar[1], G. Zoltan Laszik[2]
[1]San Francisco, CA, [2]University of California, San Francisco, San Francisco, CA

Disclosures: Vighnesh Walavalkar: None; G. Zoltan Laszik: None

Background: The role of repeat kidney biopsy (rKBx) in patients with an initial diagnosis of lupus nephritis (LN) is understudied. Guidelines for cessation or continuation of maintenance immunosuppressive therapy after the initial diagnosis of LN are not well established. In this setting, we aim to explore the significance of rKBx in these patients.

Design: An electronic search for all LN biopsies from 1/1/1998 to 12/31/2017 interpreted at our institution was performed. Research protocol biopsies were excluded. Rates of class-switching from the previous biopsy were determined. Progression of chronicity was calculated using a tiered quantitative scoring system similar to the Banff system for transplant kidney biopsies (interstitial fibrosis/tubular atrophy, glomerulosclerosis, arteriosclerosis and arteriolosclerosis; 0-3 points each, total 0-12). A “significant” progression in chronicity was arbitrarily defined as a change of 4 points or greater in the rKBx.

Results: During the study period a total of 705 LN patients underwent kidney biopsy. 118 patients (16.7%) had 2 or more biopsies (at least one rKBx). 30 patients (4.3%) had 3 or more biopsies. Using each rKBx as an “index biopsy” (n=214), class-switch occurred in 160 cases (74.8%). 33 rKBx (27.9%) revealed downgrade from a proliferative class (3 or 4) to a non-proliferative class (1, 2, 5, or 6); and 26 rKBx (22.1%) revealed an upgrade from a non-proliferative class to a proliferative class. 79 rKBx (66.9%) showed continued activity despite treatment. A significant progression in chronicity, defined above, was seen in only 38 of 118 patients (32.2%). Amongst those with 3 or more biopsies, a significant progression of chronicity was seen in only 16 of 30 patients (53.3%). Time between successive biopsies ranged from 6 months to 14 years. Follow up time ranged from 1 to 20 years.

Conclusions: rKBx were infrequently performed during the follow-up of LN patients. When rKBx were performed, they helped to accurately classify the extent and progression of disease. The majority of patients underwent class-switching, suggesting a clear role for rKBx in determining follow-up treatment strategies. The majority of rKBx revealed ongoing activity without “significant” increase in chronicity. Further studies are underway to correlate with clinical data.

1619 Fully Digitized Workflow in a Large Academic Renal Pathology Service: Moving Away from Glass

Vighnesh Walavalkar[1], Anatoly Urisman[2], G. Zoltan Laszik[2]
[1]San Francisco, CA, [2]University of California, San Francisco, San Francisco, CA

Disclosures: Vighnesh Walavalkar: None; Anatoly Urisman: None; G. Zoltan Laszik: None

Background: We briefly summarize our 4 year experience in whole slide digital imaging (WSDI), culminating in a fully digitized workflow for renal pathology sign out. Patient care, efficiency, education and quality control (QC) were emphasized.

Design: The 1st stage was the vision for digital pathology (DP) at our institution and investment in infrastructure. The 2nd stage involved establishing standard operating procedures (SOP) for histology; validation of a prospectively designed workflow using WSDI; and integration of the Image Management System (IMS) with the LIS (CoPath). In the next stage (ongoing), the actual workflow was implemented in daily renal pathology sign-out with involvement of trainees and clinicians.

Results: 2015 and prior: Funding was obtained for hardware and software for WSDI [Philips UFS scanners, computers and Image Management System (IMS)].

02/2015 - 04/2017: the SOP was optimized for the digital workflow with minor modifications in routine histology and conversion from glass to plastic coverslips that allowed rapid scanning. Strict QC measures were implemented to minimize WSDI artifacts (dust, scratching, etc). Same day TAT for a preliminary diagnosis was established at 4-5 hours (time from the morning cutoff time for receiving samples to the availability of digital images of 2 H&E and 1 PAS slides). Prospective validation of WSDI for diagnostic accuracy was carried out comparing diagnoses on 160 consecutive WSDI cases against glass slide diagnoses; diagnostic discordance with no clinical significance was noted only in one case (0.6%) due to interpretative error. The Philips IMS and the LIS (CoPath) were then integrated allowing seamless communication between the WSDI and data entry environments.

04/2017 onwards: A fully digital workflow was implemented for the renal biopsy service for primary diagnosis. This also allowed for complete digital "previewing" and sign-out with trainees, remote consultation with in-house clinicians and outside clinicians (via Microsoft Zoom), medical school education and research collaborations. Greater than 2500 cases have since been digitized and signed out using WSDI and DP.

Conclusions: Departmental and hospital support (financial and logistical), standardized histology and scanning protocols, strict QC, development of a flexible workflow, linking the WSDI system and LIS, and most importantly incorporation of opinions and ideas from trainees and colleagues were crucial for the establishment of a fully digitized workflow in renal pathology.

1620 Podocyte Expression of Mpv17l Is Downregulated in Diabetic Nephropathy

Jacob Whitman[1], Agnes Fogo[2], Haichun Yang[2]
[1]Vanderbilt University, Greenbrier, TN, [2]Vanderbilt University Medical Center, Nashville, TN

Disclosures: Jacob Whitman: None; Agnes Fogo: None; Haichun Yang: None

Background: The pathophysiology of diabetic nephropathy (DN) is not well understood. We therefore analyzed renal cortical tissue from a db/db/eNOS$^{-/-}$ murine model by RNA-seq and identified altered novel genes with human orthologs. We aimed to assess the specific localization of these genes in the kidney and determine their expression in DN in order to better understand the implications of these genes in DN pathogenesis. Amongst 529 genes that were differentially regulated in db/db eNOS$^{-/-}$ mice, we focused on 8 novel genes with similarly regulated human orthologs. Here, we present data concerning Mpv17l, which encodes for a mitochondrial protein that likely functions in reactive oxygen species metabolism, mitochondrial genome maintenance, and apoptosis.

Design: Transcription of genes of interest was assessed by Nanostring Technologies in tissue from normal nephrectomies (n=24) and DN biopsies (n=21). Morphological lesions and clinical data were assessed for each biopsy. Biopsies with mild (n=20), moderate (n=19), or severe (n=20) DN were compared to normal kidney tissue from nephrectomies (n=20) for protein expression of selected genes by IHC. Protein expression and localization were scored and compared to morphologic lesions, clinical data, and follow-up for each patient. IHC was also performed on biopsies with minimal change disease (MCD) (n=3) and primary FSGS (n=3).

Results: Downregulation of renal cortical Mpv17l transcription was significantly correlated to increased global glomerulosclerosis (GS) (r^2=0.2195, p=0.03), arteriolar hyalinosis (r^2=0.2297, p=0.03), and interstitial fibrosis (r^2=0.2118, p=0.04). In normal controls, Mpv17l was strongly expressed in podocytes and tubular epithelium. Podocyte Mpv17l expression was significantly reduced (p<0.0001) in sclerotic and non-sclerotic glomeruli in all three DN groups when compared with control. Mpv17l downregulation in podocytes was significantly correlated to increased global GS (r^2=0.177, p=0.0009) and loosely correlated to increased serum creatinine (r^2=0.0638, p=0.06). Mpv17l podocyte expression was not significantly reduced in MCD and was variably downregulated in primary FSGS. Tubular Mpv17l expression was significantly downregulated compared to control in severe DN.

Conclusions: We speculate that Mpv17l is a possible marker for podocyte dysfunction in DN and is associated with deterioration of renal function. The lack of similar downregulaton in other proteinuric conditions suggests a specific role for Mpv17l in the pathogenesis of DN.